Mississippi State University

Scholars Junction

8-7-2010

Investigation of high rate mechanical properties and damage evolution in porcine liver tissue

Joseph Chen

Follow this and additional works at: https://scholarsjunction.msstate.edu/td

Recommended Citation

INVESTIGATION OF HIGH RATE MECHANICAL PROPERTIES AND DAMAGE

EVOLUTION IN PORCINE LIVER TISSUE

By

Joseph Chen

A Thesis
Submitted to the Faculty of
Mississippi State University
in Partial Fulfillment of the Requirements
for the Degree of Master of Science
in Biomedical Engineering
in the Department of Agricultural and Biological Engineering

Mississippi State, Mississippi

August 2010

INVESTIGATION OF HIGH RATE MECHANICAL PROPERTIES AND DAMAGE

EVOLUTION IN PORCINE LIVER TISSUE

By

Joseph Chen

Approved:

_____   _____
Jun Liao   Lakiesha Williams
Assistant Professor of Agricultural and   Assistant Professor of Agricultural and
Biological Engineering   Biological Engineering
Major Professor   Committee Member

_____   _____
Filip To   Allen Crow
Associate Professor of Agricultural and   Assistant Professor of Basic Sciences of
Biological Engineering   the College of Veterinary Medicine
Committee Member   Committee Member

_____   _____
Steven H. Elder   Sarah Rajala
Associate Professor of Agricultural and   Dean of the Bagley College of
Biological Engineering   Engineering
Graduate Coordinator

Name: Joseph Chen

Date of Degree: August 7, 2010

Institution: Mississippi State University

Major Field: Biomedical Engineering

Major Professor: Jun Liao

Title of Study: INVESTIGATION OF HIGH RATE MECHANICAL PROPERTIES
AND DAMAGE EVOLUTION IN PORCINE LIVER TISSUE

Pages in Study: 93

Candidate for Degree of Master of Science

Each year, 6.4 million automobile accidents account for approximately 40,000 deaths in the United States. With increasing requirements for automobile safety, computational models capable of simulating organ deformation/ injury during high impact scenarios would be extremely valuable for optimizing safety measures. Accurate experimental data is essential for the accuracy of the models; however, there has been a sparse investigation into high-strain biomechanics which is necessary to address organ/tissue response in high impact scenarios. Damage threshold criterion and damage evolution are other areas that have not been well studied. In vehicular accidents, damage to the liver is the most common cause of death after abdominal injury. High fidelity computational modeling with damage predictor is thus capable of describing liver tissue that is subjected to blunt impact. In this study, we address high strain biomechanics and damage evolution of liver tissue in an effort to generate valuable meaningful FE models.

DEDICATION

       This work is dedicated to my father, Samuel, and my mother, Maomi. Their contributions to my life are endless, and their love and support for me are overwhelming. I thank my parents for the direction and advice given to me and the encouragement to overcome many obstacles. The love of God apparent in their lives has truly given me the strength and motivation to succeed. To my brothers, Tim and Michael, for their steady support and love. Their companionship with me from past to present is a true blessing.

ACKNOWLEDGEMENTS

TABLE OF CONTENTS

LIST OF TABLES

LIST OF FIGURES

CHAPTER I

INTRODUCTION

1.1 Automobile Accidents

It is estimated that automobile accidents lead to the death of 1.2 million people worldwide each year and cause injury of some sort to 50 million more people [1]. It is involved in 2.2% of all deaths in the world and is the leading cause of death among children 10-19 years old worldwide [2]. In the United States, it is the 6th leading preventable cause of death with approximately 46,000 deaths and 2.4 million injuries [2, 3]. Not only are automobile accidents detrimental to the well being of the human body, it also contributes to significant financial costs to society and the individual.

Figure 1   Automobile accident involving a side impact collision; From (Howard)

The first recorded death attributed to an automobile accident occurred on August 31, 1869 when Mary Ward of Ireland was run over by an experimental steam car built by her cousins [4]. The first North American death came thirty years later on September 13, 1899 when Henry Bliss was hit after stepping off a New York City trolley [5]. Today, more than 20 million people have died from automobile accidents.

As cars became commercialized around the 1930s, deaths from automobile accidents increased steadily. Automobile safety was largely disregarded for most of the 30s, 40s, and 50s. With rigid components and protruding knobs, buttons, and levers, the cars of that time led to a high chance of serious injury or death [6]. Car manufacturers in the 50s even claimed that vehicle accidents were simply too vigorous for humans to survive [7]. Eventually, the need for automobile safety became too great to be neglected anymore.

1.2 The Evolution of Automobile Safety Testing

1.2.1 Cadaver Testing

Around the late 1950s, Cadaver testing at high impact scenarios began at Wayne State University in Detroit, Michigan [7]. This marked the first time serious scientific work was done to improve safety in automobiles. Cadavers were used to investigate the human body response to high speed incidents [8, 9]. Researchers dropped cadavers down elevator shafts, hit them with steel ball bearings, and subjected them to automobile crashes such as rollovers and head on collisions [10]. Accelerometers were placed on the cadavers during these scenarios, and data was obtained that allowed researchers to determine safety measures.

2

Cadaver testing contributed much to the advancement of car safety; however, moral and ethical concerns along with some research limitations eventually led to the discontinuation of cadaver testing [11]. Limitations included the skewed sample population in that the cadavers used for testing were mostly elderly individuals; a proper demographic population could not be attained.

1.2.2 Volunteer Testing

Some researchers also took it upon themselves to subject their bodies to traumatic force. A particularly famous researcher, Colonel John Paul Stapp, strapped himself to a rocket sled that traveled at 1000 km/hr and came to a complete stop in 1.4 seconds to study the effects of this rapid deceleration on the human body.

Figure 2   Example of Volunteer Testing in High Impact Scenario; Colonel John Paul Stapp in a rocket sled; from [6]

Dr. Lawrence Patrick of Wayne State University subjected himself and his students to various sorts of impacts including heavy metal pendulums to the chest, pneumatic powered hammers to the face, and shattering glass [7, 12]. Dr. Patrick claimed these types of tests created valuable data that could be used to generate mathematical models; however, these types of impacts were too minor to cause serious injury and give insight towards the human body response to high impact scenarios.

1.2.3 Animal Testing

Animal testing became the next area of interest particularly because animals were alive and could give researchers a connection between force and survivability (Figure 3).

The most common animal used was the pig because its internal structure was similar to humans. During the *Eighth Stapp Car Crash and Field Demonstration Conference*, Mary Roach gave the public an insight into animal testing. "We saw chimpanzees riding rocket sleds, a bear on an impact swing...We observed a pig, anesthetized and placed in a sitting position on the swing in the harness, crashed into a deep-dish steering wheel at about 10 miles per hour." [12]

Figure 3   Example of Animal Testing in High Impact Scenarios; From [10]

Animal testing contributed greatly to the progress of car safety, but it did run into much controversy. Many groups, such as the American Society for the Prevention of Cruelty to Animals (ASPCA), strongly protested against animal testing and eventually led to the discontinuation of animal testing altogether [10]. However, by this time, many tolerance levels for injury were determined from this research.

Although animal testing significantly benefitted researchers understanding of traumatic injury, there were still major limitations. Animal subjects still differed greatly from humans particularly in their bone structure and organ organization. More human-like specimen devoid of ethical issues must be used to fully understand the mechanisms involved in automobile accidents.

1.2.4 Dummy Testing

The need for reproducible and non controversial experiments came in the form of crash dummies around 1949. Sierra Sam, created by Samuel W Alderson, was the first dummy used for determining safety measures (Figure 4) [13].
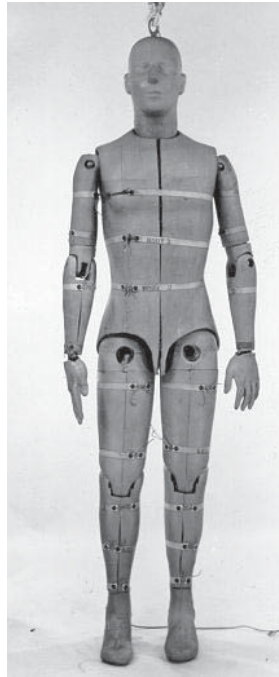
Figure 4   Sierra Sam Dummy manufactured by Sierra Engineering Co; From (Seed)

He was used primarily for the testing of aircraft ejection seats and pilot restraint harnesses. Alderson and Sierra Engineering Co. both submitted dummies, the VIP-50 series and Sierra Stan respectively, to General Motors (GM) and Ford to be used in car crash scenarios, but General Motors decided to develop its own dummies for car crash testing [13]. In 1971, GM unveiled the Hybrid I dummy which was also known as the "50th percentile male" dummy [14]. Hybrid I was designed to model an average male in height, mass, and proportion. As the first version, there were many improvements to be made and within a year Hybrid II was released (Figure 5).

Hybrid II provided better shoulder, spine, and knee responses. It was the first dummy to achieve consistent results and good durability. Similar to Hybrid I, Hybrid II mimics the size and range of motion for the 50th percentile male [13, 15].

Figure 5   Hybrid II Dummy manufactured by First Technology Safety Systems;
             From [15]

It is composed of an internal superstructure made of a variety of materials (steel, aluminum, brass, delrin) to simulate bone structure. Outer materials include a vinyl combination and foam materials. In 1973, it was the first dummy to be approved for testing of seat belts by the American Federal Motor Vehicle Safety Standard (FMVSS). Although much improvement was made on the Hybrid II, it was still very basic and could only be used to evaluate a small range of injuries.

Hybrid III was released in 1976 and is now the most widely used crash test dummy in the world [16]. It is considered to have the highest biofidelity of any existing dummy [15, 17]. The Hybrid III has improved responses from the head and neck, upper torso, and lower torso. With a rubber and aluminum neck, it accurately simulates the

8

motions involved in the neck (dynamic moment/rotation flexion and extension). The upper torso is composed of six steel ribs that connect to a spine and simulates chest force deflections. The lower torso includes detailed parts that even simulate hip to leg and foot to ankle motions. Overall, the Hybrid III is a very detailed piece of equipment that is being continually improved.

Figure 6   Family of Hybrid III Dummies designed to consider the entire general
               public; From [15]

Further improvements included the design of a Hybrid III family (Figure 6). The first Hybrid III dummy was the 50th percentile man which was 175 cm (5' 9") tall and weighed 77 kg (170 lb). His big brother, the 95th percentile man, was 188 cm (6' 2") tall and weighed 100 kg (223 lb). The 50th percentile Hybrid III had a wife, the 5th percentile female, who was 152 cm (5') tall and weighed 50 kg (110lb). There were also three

children dummies representing a ten year old, a six year old, and a three year old. The children dummies height and weight were: 32 kg (71 lb), 21 kg (41 lb), and 15 kg (33 lb) respectively [13, 15, 17].

Although the Hybrid III made drastic improvements to car safety, it was still limited because it was designed to simulate frontal impacts. As researchers progressed the field of dummy testing research, they realized new dummies needed to be designed to specifically address the different types of impact. Different dummies were designed to evaluate side and rear impacts [13, 15]. The Side Impact Dummy (SID) specifically investigates the rib, spine, and internal organs in side collisions. The Rear Impact Dummy (RID) is interested in assessing whiplash in passengers from rear collisions [18, 19]. Other dummies include the Child Restraint Air Bag Interaction (CRABI) dummy which assessed infants and the safety of car seats. The CRABI dummy considers three age groups: 6 month, 12 month, and 18 months. More recently, the Maternal Anthropometry Measurement Apparatus Version 2B (MAMA2B) dummy emerged for representing pregnant women in automobile accidents [15]. All of these new types of dummies aim to represent the normal demographic of any human society.

Figure 7   MAMA2B Dummy designed in consideration of the pregnant
             population; From [15]

As dummies become more advanced, more safety concerns are addressed and it is apparent in the safety features of new automobiles; however, the fact is that although automobiles are safer now than they ever were, the number of fatalities related to car accidents each year is still very high. One major concern is that dummies do not respond to impact as humans do in certain regions. Bodily organs such as the brain and abdominal organs are not investigated in dummy research. Also, simple force thresholds are not sufficient to address organ damage and other factors involved in automobile accidents that contribute to death of the patient. Furthermore, the Federal Motor Vehicle Safety Standard (FMVSS) only deems it necessary to tests impacts up to 30 miles per hour [20]. This standard speed is not realistic to many automobile accidents which occur

at much high speeds. Seeing the need for optimizing the protocols for evaluating safety in automobiles, researchers have shifted the direction of research towards Finite Element (FE) modeling [21].

1.3 Finite Element Method

As real-world engineering problems became increasingly complex, the need for methods capable of analyzing these problems became apparent. The theory and development of the finite element method can be traced back to the work of Alexander Hrennikoff and Richard Courant in the 1940s [22]. By the late 1950s, the finite element method began to be applied to aerospace and civil engineering problems and much progress was made at the University of Stuttgart and University of California-Berkeley. In the 1960s, NASA wrote proposals for the development of a finite element software called NASTRAN. FEM eventually became established when William Strang and George Fix published the book *An Analysis of The Finite Element Method* in 1973 [23]. Since then, FEM has become vastly improved due to the advanced capabilities of computers. FEM software such as ABAQUS and ANSYS has become widely used in the academic and industrial world [24].

Figure 8   Finite Element Method simulation describing the impact of an
            automobile with a rigid object; From (Rahmm Tech)

The concept of FEM begins with a governing differential equation [25]. This equation describes a phenomenon of interest in mathematical form. The derivation of this equation can be formulated by a combination of many accepted laws or equations such as the principle of conservation of linear momentum (Newton's second law), or the second law of thermodynamics to name a couple. The process of FEM involves solving differential equations via numerical simulations which utilize numerical methods in conjunction with computers to provide approximate solutions. Numerical methods solve differential equations by transforming a differential equation into a set of algebraic equations. Several numerical methods exist such as the finite difference approximation method and classical variational methods.

In the finite difference method, the derivatives in a differential equation are replaced by difference quotients which cause it to be algebraic. The algebraic equation represents the governing equation at a certain point or time step. In order to fully summarize the governing equation, the algebraic equations must be solved at every point or time step. After imposing initial-value conditions or boundary-value conditions, the governing equation in algebraic form can be solved to describe the governing equation at hand. The finite difference is a very useful tool, especially in simpler scenarios; however, as the geometries get more complex, the finite difference method become less attractive.

Classical variation methods include the Ritz, Galerkin, collocation, and least squares method. These methods differ from each other by integral form, weight functions, and/or approximation functions. Classical variation methods take a governing differential equation and convert it to an equivalent weighted integral form, allowing it to be solved and manipulated with the concepts of linear algebra. The solution, or right hand side of the equation, is assumed to be a linear combination of chosen approximation functions and undetermined coefficients. The undetermined coefficients are solved as an approximation solution for the differential equation.

The finite element method utilizes the classical variation methods approach, but converting a differential equation describing a physical phenomenon to the weak integral form. The process of FE can be described in three steps.

1. Depending on the geometric complexity of the material of interest, discretize it into many geometrically simple elements. Discretization can also be described in

this fashion. The whole geometric shape can be thought of as the domain. The domain is to be divided into many smaller, simpler subdomains.

2. Over each subdomain, or finite element, the governing equation in weak form is assigned over the subdomain at its nodes.

3. Each element is assembled back into the global domain with boundary conditions between each element being satisfied. With the global domain assembled and the governing equation assigned, the full analysis of the material is possible.
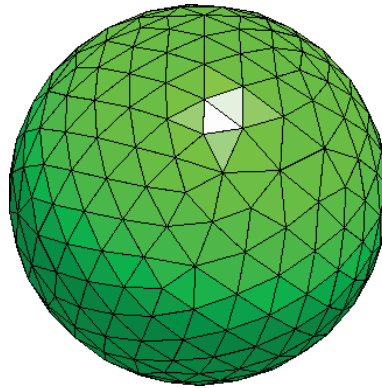
Figure 9   Discretization of Ball for FE applications; From (NMAG)

To reiterate, consider the example of a ball being thrown against a wall. The domain of the geometry would encompass the whole ball. In order to describe it in terms of its subdomain, discretization must be done. Discretization is also termed meshing in finite element terminology. Meshing a geometry would divide the ball into multiple subdomains or elements. These elements are much simpler geometrically. Each triangular element will possess the material properties and the governing differential equation of the scenario that we are investigating. In terms of throwing a ball, one would

likely use Newton's second law to determine the forces that the ball will experience during impact into a wall. After determining and assigning the governing equation, one must assign boundary conditions such as speed of the ball and the material properties of the wall that is being impacted. Each element is analyzed and assembled back together with the correct boundary conditions. The simulation can now be run. After the simulation outputs the data, the model must be validated. Validation involves comparing the outputted data with real world experimental data. This is also a major concern in that it involves the accuracy of the simulation. In many real world problems, validation is often a complicated procedure. After validation, the simulation can be run infinite times and the parameters can be adjusted as desired.

In simple scenarios such as heat transfer through a rod, FEM can allow users to see the progression of heat at each point of the rod and give detailed insight without much computational burden. However, when FEM gets applied to more complex systems with highly irregular geometry shapes, the computation load becomes tremendous. Therefore, much of the success of FEM relies on the technology that is available. Thankfully, in the recent decade, computers have advanced at such a rapid rate that much of these simulations can be run in a reasonable amount of time.

FEM simulations in the real-world can become especially complicated as researchers investigate very specific scenarios. The worth, however, is great because FEM simulations can accurately represent scenarios that would either be very expensive to simulate or too dangerous to implement in the real world. In regards to this thesis, FEM simulations would be extremely valuable for investigated automobile accidents.

The time saved because of FEM simulations is great and the money saved would be even greater.

1.3.1 FEM for automotive industry

Specifically for investigating automobile accidents, increasing efforts are being placed on generating an accurate FEM model [26]. King et al. discussed the feasibility of utilizing models to represent high impact trauma in humans [27]. Kirkpatrick et al. actually generated a FEM model of the SID dummy to assess the dummy in a simulation [28]. The model response was compared to experimental results to see if the simulation was feasible. Although, these preliminary models accurately simulated a dummy's response to a high impact scenario, their worth to improving car safety is limited [29]. These simulations allow researchers to observe the response of a dummy; however, the dummy's response is obviously different from that of a human. If one were able to input a FE model of a human being into the simulation, the value of that simulation would be tremendous. The recent direction of the field is just that: generate a FE human body model.

Jost et al presented a preliminary model of an FE human body model [30]. They created a model that contained detailed biomechanical data concerning bones and stiffer bodily structures, but they were not able to characterize the soft tissue. Zhao et al created a more detail model simulating the body regions of the thorax, abdomen, should, and head-neck [31]. More recently, Fressmann et al introduced the Total Human Model for Safety (THUMS) model [32].

17
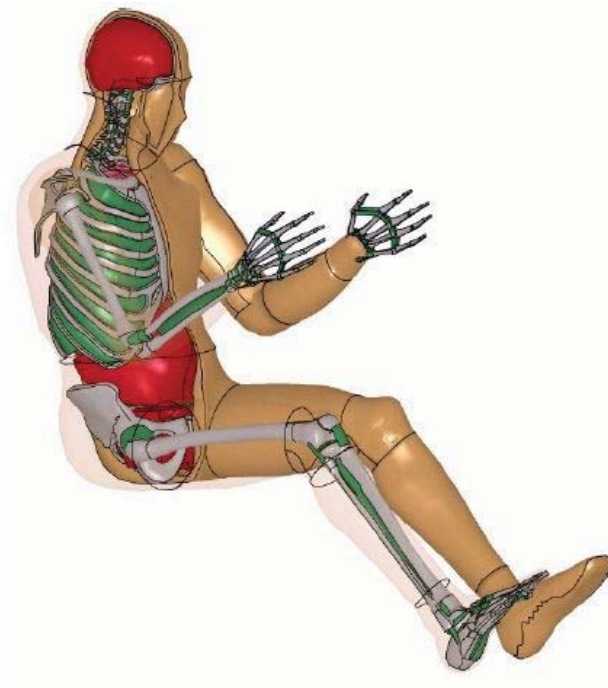
Figure 10   THUMS FEM Model present by Fressmann et al.; From [32]

This model captured a human response relatively well, but the authors acknowledged many of its shortcomings and shared future insights in improvements that must be made. Some concerns were that some of the organs were modeled as groups, and they represented a general response not specific to each organ. Other concerns dealt with the lack of considering muscle activity in the model. Overall, the authors recognized the complexity of the human body and the amount of research that must be done to achieve the ultimate goal of an accurate FE model of the human body.

1.4 Abdominal injury: Liver

As researchers aim to develop meaningful FE models, accurate data concerning each organ must be experimentally investigated. The liver is the most commonly injured abdominal organ in automobile accidents; also, liver damage causes the highest mortality rate in traumatic injury cases [33-37]. Characterizing the liver will contribute to the generation of a FE human body model and will also benefit liver trauma/liver disease research in that these models can potentially be used in robot assisted surgeries. In this study, the liver was chosen because of its prevalence in abdominal injuries in automobile accidents[38].

The human liver is the largest organ in the body [39]. It contributes to roughly 1/50 of one's body weight and contains around 50,000 to 100,000 individual lobules. Structurally, the liver consists of lobules, which are cylindrical structures several millimeters in length and 0.8 to 2 millimeters in diameter. Each lobule surrounds a central vein and consists of hepatic cellular plates which are about two cells thick and organize themselves in a fashion that resembles spokes on a wheel. Each cellular plate contains bile canaliculi which empty into bile ducts. Each lobule is separated to each adjacent lobule by fibrous tissue (septa).
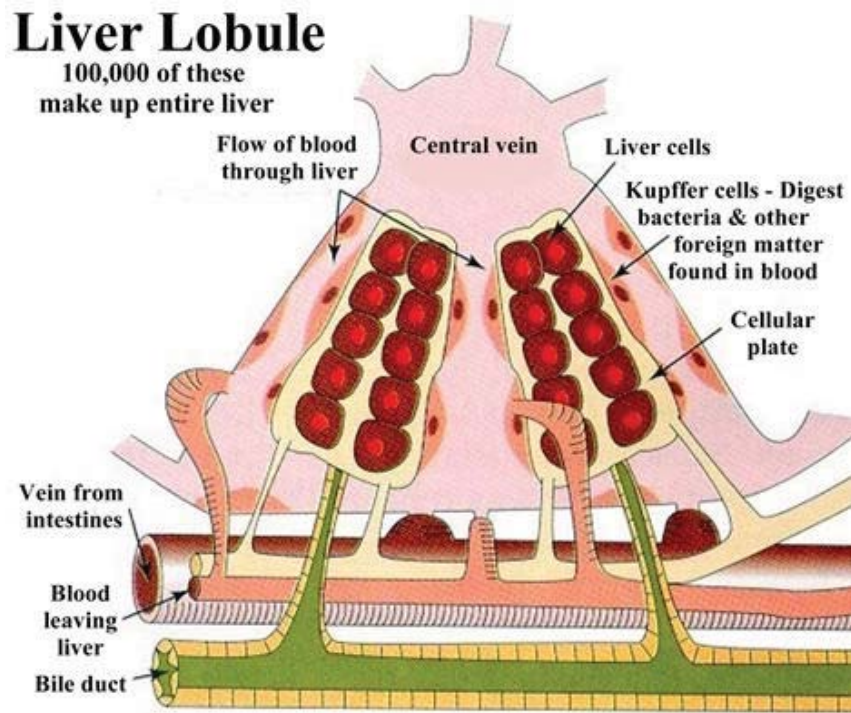
Figure 11   Diagram of Liver Lobule [39]

Functionally, the liver receives its blood supply primarily through the portal venules and the hepatic arterioles. Blood flows through the lobule by way of hepatic sinusoids and into the central vein. By flowing in this way, all the hepatic cells are exposed to the blood and are able to contribute in many important processes which will be discussed later. In addition to hepatic cells, there are two other types of cells: endothelial cells and large Kupffer cells. Endothelial cells line the walls of the blood vessels and prevent coagulation and clot formation, and Kupffer cells phagocytize bacteria and other foreign substances in the blood.

The liver serves many important functions such as: carbohydrate metabolism, fat metabolism, protein metabolism, filtration of harmful substances, storage of vitamins, maintenance of proper glucose levels in the blood, and the formation of coagulation factors. The structure and cellular make up of the liver allows blood to pass through a certain path that allows all the blood to be filtered in a synergistic fashion. With various vital functions of the liver, the importance of the liver as an organ is evident.

1.5 Motivation, Rationale, and Specific Aims

As we mentioned above, automobile accidents lead to 1.2 million deaths and 50 million injuries world-wide each year. It is considered the 6th leading preventable death in the United States. Furthermore, liver injury contributes to 30% of all deaths relating to trauma. Although much improvement has been made in automobile safety, there continue to be a large number of deaths attributed to it each year. Also, the injuries sustained from automobile accidents can be serious and cause much physical and emotion strain to its victims. As car safety research has progressed, there has been a great desire for FE simulations of a human body in high impact scenarios. Not only would these simulations reduce the cost of safety testing, they would also increase the accuracy of the data generated and allow researchers to optimize the safety features of any conventional automobile.

There are significant limitations in the current human FE models. The main concern involves validation. Validation involves comparing a model's response to a force or stimuli to the real world response of the same force or stimuli. Furthermore, validation involves the investigation of the accuracy of the real world data. The problem

for current models is that the real world data that exists for the human body at high impact scenarios is not completely accurate.

Human models in the past have utilized pendulum tests to validate a body region's response to impact. Viano et al used a 23.4 kg 15cm flat circular pendulum to impact cadavers at different regions [40, 41]. Researchers would then investigate the damage that occurred (cracked ribs, lacerated organs) and determine a threshold criterion for acceptable force. The study considered the cause and effect of a certain force, but neglected to understand how the damage progressed or occurred. Therefore, current models used these threshold values to indicate damage. There are two main problems with using this data for modeling. Firstly, there is a lack of understanding for the responses of the organs which is an area of concern because often times deaths occur from the rupture of an organ. An accurate assessment of each organ would generate a more detailed model that will allow for better elucidations for car safety. Secondly, there is a lack of understand of damage. A simple cause and effect approach is too general to investigate damage thresholds for high impact scenarios.

In this study, we aim to: (1) accurately assess the liver organ by using high strain rate mechanical testing, (2) offer an approach for quantifying damage by utilizing interruption testing and histological analysis, (3) establish methodologies for high strain rate tissue biomechanics and damage evolution modeling.

Specific Aim 1: Accurately assess the liver organ by using high strain rate mechanical testing. In order to generate an accurate FE simulation of the liver in a high impact scenario, the inputted data must represent the organ's response in a high impact fashion. It is accepted that soft tissues are strain rate dependent; however, in the majority

22

of FE simulations, quasi static biomechanical data is used as inputted data for FE simulations. The result of this is an inaccurate model, unable to simulate the true response of the organ in deformation. High strain biomechanics of soft tissue is a new avenue in biomechanics and is one that has not been thoroughly investigated; however, it is necessary for the production of an accurate FE model. By applying the Split Pressure Hopkinson Bar testing, which has been established as a methodology for testing metals at high strain rates, we aim to establish a protocol for high strain rate testing of soft tissues. The ultimate goal is to generate accurate high strain rate biomechanical data for the liver in hopes of creating an accurate FE model for automobile accidents.

Specific Aim 2: offer an approach for quantifying damage by utilizing interruption testing and histological analysis. When an accurate FE simulation is produced, there is yet still an area of uncertainty; the question being "where is the threshold for damage/deformation?" Damage has not been objectively studied and often threshold values for these models are assumed from cadaver impact experiments. These cadaver impact experiments are limited because of its cause and effect approach which could lead to a high error. We aim to introduce an interruption testing approach which will allow us to study the microstructural change that occurs with increasing strain. By utilizing image analysis software, we are able to analyze damage trends and generate constitutive models and ultimately FE models that will be able to describe in an objective way the evolution of damage. With this detailed information, research will be able to conclude to more accurate thresholds of damage from the FE simulations.

Specific Aim 3: establish methodologies for high strain rate biomechanics and damage evolution modeling. As the need for more advanced and precise FE models

becomes greater, new and more detailed methodologies must be produced to meet the requirements of the next level of models. High strain rate biomechanics of soft tissue is still in its infant stages, and we aim to contribute greatly to the advancement of this field. In establishing a thoroughly investigated, accepted method, researchers will be able to apply this method and generate data for other organs and expedite the process for characterizing all organs of the body. Furthermore, establishing an approach to damage modeling will also allow researchers to better understand damage in soft tissues and also various organ types. Ultimately, the result will ideally be a collaborative environment that will issue into the production of a highly precise FE model, which is able to describe the true response of the human body in an automobile accident and other high impact scenarios.

CHAPTER II

MECHANICAL RESPONSE OF PORCINE LIVER TISSUE UNDER HIGH STRAIN

RATE COMPRESSION

2.1 Introduction

The liver is the most frequently injured intra-abdominal organ [33]. In 2007, 1.7 million car accidents in the United States resulted in injury (National Highway Traffic Safety Administration), and one of the most commonly injured abdominal organs in motor vehicle accidents is the liver [42, 43]. Regarding the assessment of automobile-related accidents, since the late 1970s, crash dummies have been utilized to determine optimal safety measures [44]. The injury metrics for dummies in car crash scenarios are typically force and acceleration. Injury assessment reference values (IARV) were first proposed by General Motors for dummies in crash tests and were determined so as to define a tolerance level of 5% significant injury risk of various organs [45, 46]. However, an improved, more cost-effective alternative to assess organ damage during car crash situations is the development of computational models that can represent the human body in more detail and are able to more accurately predict the risk of human tissue/organ injuries. Recent work in developing a geometrically correct "virtual human" has been performed with the goal of measuring bodily trauma in automobile accidents [47-50]. However, soft tissue material properties so crucial to a precise human model are currently lacking.

The development of an accurate computational model requires knowledge of the mechanical properties of many human tissues and organs under different loading conditions, especially in high-impact situations. Quasi-static biomechanical characterizations of soft tissues have been performed since the 1970s to determine the mechanical properties of various tissue types [51-56]; however, regarding the response of tissues that may be subjected to high-impact situations such as automobile accidents, sport injuries, and blunt trauma, these quasi-static tests are limited and cannot be extrapolated to high rate applications. Because soft tissues are strain rate sensitive, mechanical testing thus must be performed at higher strain rates to properly describe the tissue's response during blunt force impacts.

For high strain rate mechanical testing on liver tissues, a standard protocol has not been well established. Researchers have utilized different apparatuses to perform high strain rate testing. Sparks et al. built a drop tower in which a weight was dropped onto a whole human liver organ, resulting in average strain rates up to 62 s^{-1} [57]. Others have used indentation instruments to generate strain rates up to 200 s^{-1}. In hopes of establishing a methodology of high strain rate testing, we considered the split Hopkinson pressure bar (SHPB) apparatus. The SHPB has the ability to apply compressive stresses at high strain rates (100–10,000 s^{-1}) [52] and has been widely applied in metal mechanics [58-61]. Elastic wave propagation in the SHPB system can be analyzed based on the principle of superposition of waves and the elastic wave propagation theory of classical mechanics. As a result, the stress, strain, and particle velocity can be estimated by analyzing the incident wave and reflected wave at any cross-section [62].

When the SHPB is used for testing soft tissues, many issues must be considered to generate consistent, accurate data. Recently, the incorporation of polymeric bars into the SHPB setup has allowed for testing of soft materials such as rubber and biological tissues, of which the acoustical impedance matches more closely with that of the softer polymeric bars. Unlike conventional metallic bars, polymeric bars enable a smooth passage of energy generated by the impact of the incident bar and the soft specimen, resulting in smoother, more noise-free curves [51]. A few groups have applied the SHPB apparatus for soft tissue biomechanics experimentation. Song et al. tested porcine muscle along two perpendicular directions at dynamic strain rates up to 3700 s^{-1} using the SHPB and found that both directions showed a nonlinear, strain rate dependent behavior [51]. Similarly, Van Sligtenhorst et al. found the mechanical response of bovine muscle at strain rates up to 2300 s^{-1} with the polymeric SHPB to be strain rate dependent [52].

The objectives of the present work are (i) investigate the tissue behavior of porcine liver at high rate impacts using a custom-made PSHPB coupled with finite element analysis and (ii) establish appropriate protocols for testing soft tissues using the PSHPB method. Both experimental results and computational simulations of liver tissue under high strain rate conditions will be incorporated into a human model, which in the future will be implemented to optimize safety measures that could reduce the risk of human injuries and death in high-impact situations.

2.1.1 Biomechanics

A detailed evaluation of biomechanics and its current limitation is important for a proper understanding of the need for high strain biomechanics. Biomechanics can simply

27

be defined as mechanics applied to biology [63]. It has been an essential pillar for the progression biomedical engineering and continues to do so today. It aims to help researchers understand normal function of the body, predict changes due to alterations, and propose new methods of educated intervention. By evaluating the properties of various tissues, many conclusions and constitutive equations can be determined. Constitutive equations of the material properties of various biosolids can only be developed with accurate experimental analysis.

The simplest biomechanical test that can be performed is uniaxial tension or compression test. By applying a load to a certain tissue, one can extrapolate meaningful data in the form of a stress-strain curve. This approach has been applied to a variety of different organs, tissues, and even individual extracellular matrix components (e.g. collagen). Information regarding the material property of the tissue of interest include tangent modulus, ultimate failure strength, hysteresis, and many others. Generally, stress strain curves can describe how ductile or brittle, strong or weak, a tissue is.

It has been shown that all soft tissues are strain rate dependent [64]. This refers to the speed of the displacement during a test. For example, as a specimen is pulled in tension at various speeds, the response or stress-strain curves of these samples will differ significantly. Many researchers have investigated organs/tissues at low strain rates. This area of research is termed quasi static biomechanics. There has been an abundance of work in this area, and quasi static biomechanics has been applied to virtually all areas of the body. Constitutive equations have been developed in many experiments and models have been generated for the purpose of understanding mechanisms and also applications towards robot assisted surgeries. In many cases, these models are accurate and very

28

useful; however, because of the strain rate dependency of soft tissues, these constitutive equations cannot be applied to higher speed scenarios. In high speed situations, the organ response and deformation would differ greatly from the quasi static response. Significantly different stress strain curves will be generated from high strain rate biomechanical tests and therefore will require new constitutive equations to fit the high strain response. Constitutive equations are governed by the accuracy of their experimental data; and therefore, for our purpose in modeling the liver in high impact scenarios, we must determine an experimental procedure that can characterize the liver at a high strain rate.

High strain rate biomechanics is an emerging field in biomechanics. There have been few studies on the high strain rate response of various tissues. As mentioned earlier, different research groups have approached this type of testing differently, each with its limitations. Since this area of research is on the frontier of biomechanics, there are many issues and questions that must be thoroughly analyzed with a collaborative mind. We aim to establish a methodology in the Split Hopkinson bar with the knowledge laid down by previous research groups.

2.2 Methodology

2.2.1 Sample Preparation

Porcine livers from healthy adult pigs were obtained from a local abattoir. The specimens were stored in phosphate buffered saline (PBS) at 4°C soon after extraction and transported to the laboratory. All testing was performed within 12 hours of extraction. For PSHPB application, the tissue sample should be carefully extracted to a

certain shape and size. A relatively large diameter is important to ensure that most of the energy is transmitted through the sample [52]. Testing was performed on samples with aspect ratios ranging from 1:1 to 3:1, and it was determined that an aspect ratio of 3:1 produced consistent data. Thus a cylindrical die of 30 mm inner diameter was used to cut disc-shaped samples to approximately 27 mm in diameter and 9 mm thick for an aspect ratio of 3:1 (Fig. 12). The axis of the disc-shaped sample was aligned along one of the three orthogonal directions.
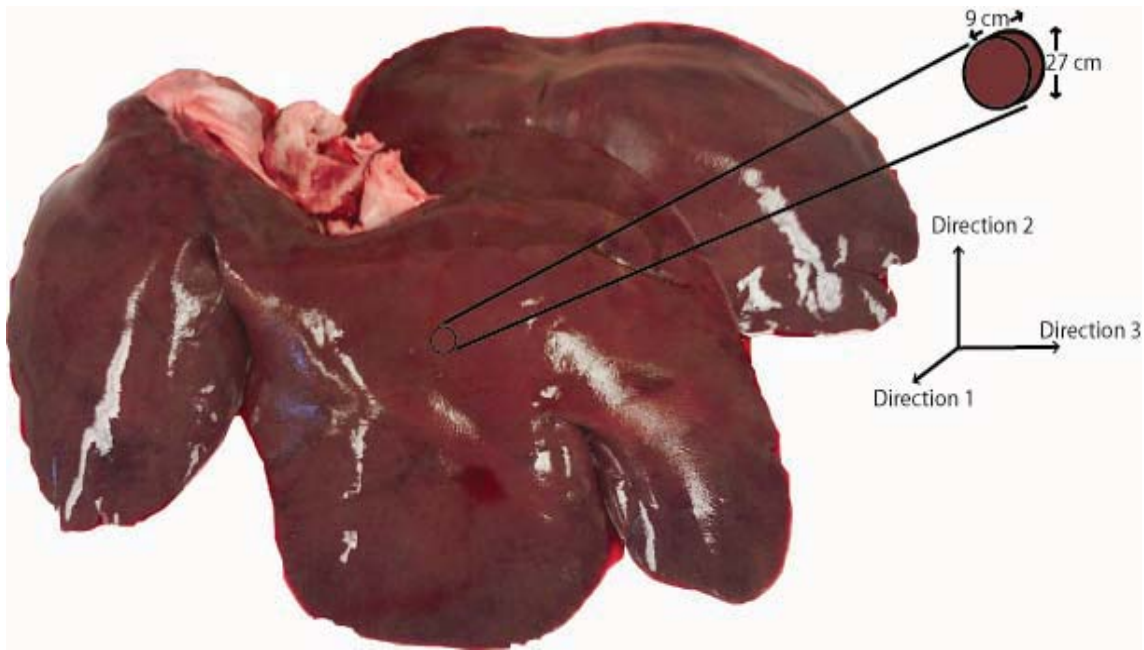
Figure 12   Three orthogonal directions (1, 2, and 3) based on porcine liver
             anatomy. Representative sample geometry and size.

2.2.2 High Strain Rate Testing using PSHPB

The PSHPB, made of commercially extruded natural polycarbonate (PC 1000) rods, is composed of a striker bar, an incident bar, and a transmitted bar with lengths 0.762, 2.438, and 1.219 m, respectively, and diameter 38.1 mm (Fig. 13).
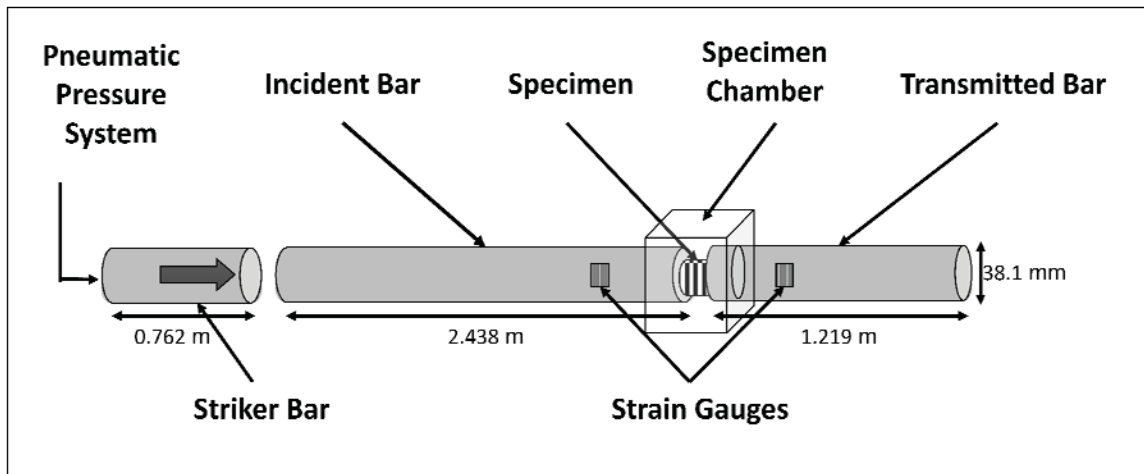
Figure 13   Schematic of polymeric split Hopkinson pressure bar (PSHPB) apparatus.

A cylindrical specimen is placed between the incident and transmitted bars, and the striker bar is propelled at a specified velocity by means of a pneumatic pressure system. As the striker bar impacts the incident bar, a compressive wave (incident wave) is generated and propagates down the incident bar where it reaches the specimen, causing compression of the specimen. At this point, a portion of the wave is reflected back into the incident bar as a tensile wave (reflected wave). The remainder of the compressive

wave (transmitted wave) is transmitted through the specimen and into the transmitted bar (Fig. 14).
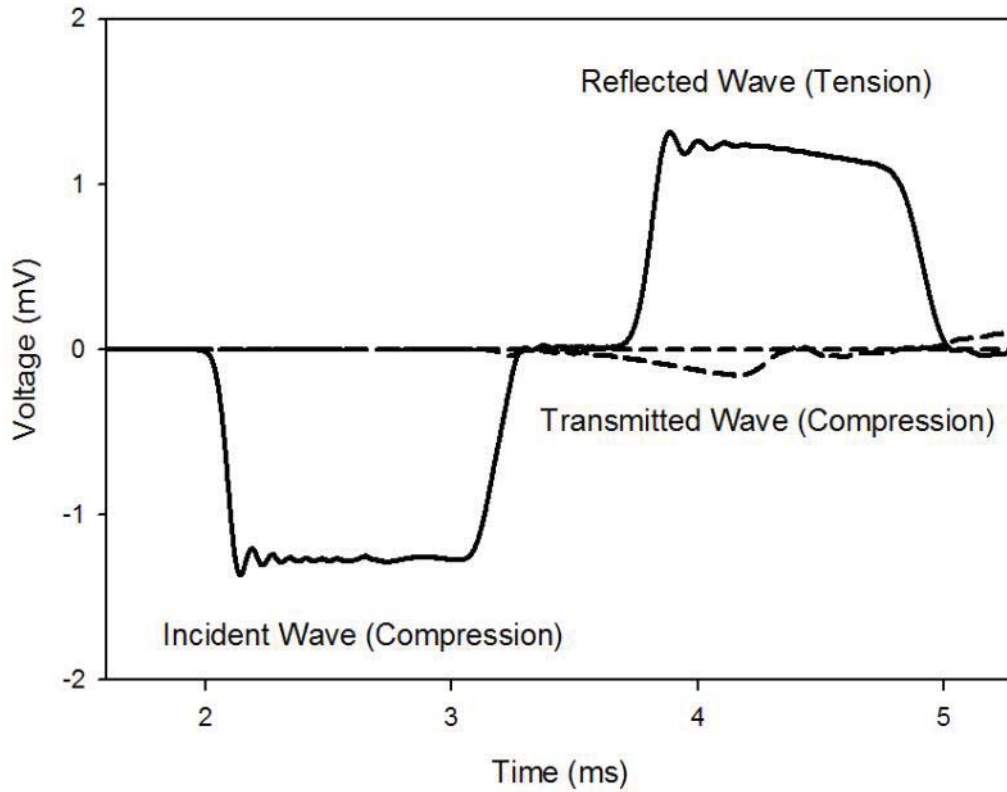
Figure 14   Incident, reflected, and transmitted waves obtained from PSHPB testing on porcine liver tissue.

The incident, reflected, and transmitted waves are measured by two strain gauges, one on both the incident and transmitted bars. The PSHPB experimental setup is based on the following assumptions: (i) the specimen undergoes uniform and uniaxial stress during deformation; (ii) the incident and transmitted bars are elastic; (iii) the edges of the bars in contact with the specimen remain flat and parallel; (iv) the incident, transmitted, and

reflected waves undergo minimal dispersion as they travel along the bars; and (v) strains measured at the surface of the bars are indicative of those throughout the cross-section (Subhash, 2000). The experimental setup also includes a laser speed meter for monitoring the incident bar speed and DAQ modules for data acquisition. Data was processed via David Viscoelastic Software [62].

Cylindrical samples were extracted from three orthogonal directions based on porcine liver anatomy (Fig. 12). For evaluating strain rate sensitivity, samples were extracted along Direction 1 (Fig. 12), and strain rates of 350 s^{-1} (n=4), 550 s^{-1} (n=4), 1000 s^{-1} (n=4), and 1550 s^{-1} (n=5) were applied. To evaluate directional dependence (anisotropy) of tissue behavior, samples were dissected along three orthogonal directions (Directions 1, 2, and 3; n=4 for each direction) and tested at a strain rate of 350 s^{-1}. For each test, a sample was glued between the incident and transmitted bars using cyanoacrylate glue (Cemedine, Japan) [65, 66]. Liver tissue was kept moist with PBS throughout the testing procedure.

2.2.3 Microstructural Analysis

To assess the microstructural characteristics of liver tissue along different orthogonal directions, samples were dissected along each orthogonal direction (1, 2, and 3), corresponding to the orientation of samples used for high strain rate testing. Liver samples were fixed in 10% neutral buffered formalin and dehydrated in a graded ETOH series. Samples were then embedded in Paraplast with CitriSolve as a transitional fluid, sectioned to a thickness of 7 μm, and subjected to Hematoxylin & Eosin (H&E) staining.

In H&E staining, liver cell nuclei were stained black/purple and extracellular matrix proteins pink.

ImageAnalyzer v.2.2-0 software (CAVS, Mississippi State University) was used for microstructural analysis of histological images from samples cut along each orthogonal direction. The parameters obtained for each image during analysis included the following: object count, cell nuclear density, area fraction of cell nuclei, mean area of cell nuclei, and mean nearest neighbor distance (nnd). Total cell nuclei area is a measure of the total area of all cell nuclei, and area fraction is the ratio of total cell nuclei area to total image area. Mean area represents the average area of cell nuclei, and object count is the number of nuclei present in the image. Cell nuclear density equals the object count divided by the total image area. Mean nnd is a measure of the average distance between neighboring nuclei.

2.2.4 Finite Element Modeling

Finite element (FE) simulations (ABAQUS 6.9) for porcine liver high rate tests were conducted to better understand the behavior of the liver tissue under high rate compression. The hyperelastic and inelastic behavior of liver tissue was fitted with a phenemological internal state variable (ISV) material model developed by Bouvard et al. (MSU TP, Ver. 1.0) [67]. The MSU TP model consists of a nonlinear Maxwell element (Branch A, non-equilibrium component) describing the time-dependence behavior, connected in parallel with a Langevin spring (Branch B, equilibrium component) representing strain hardening at large strains [67] (Fig. 15).
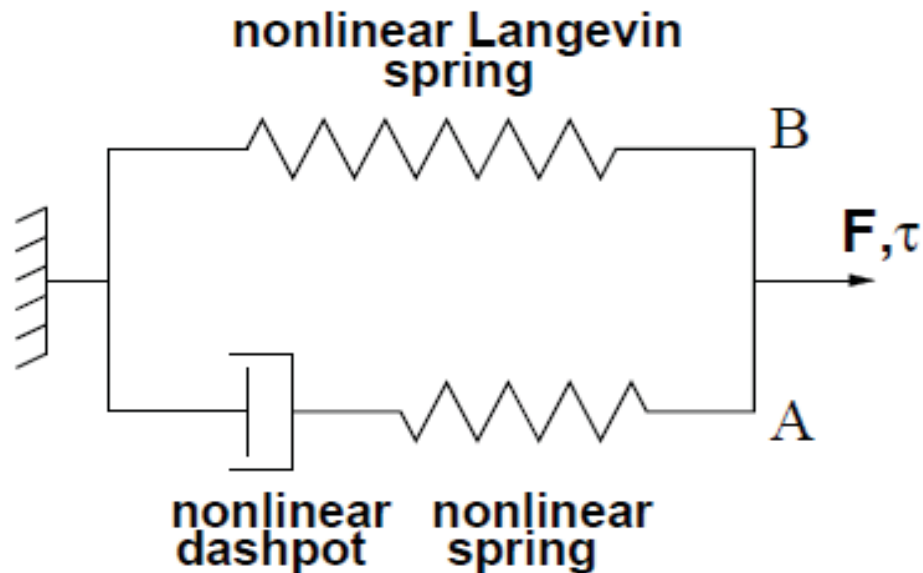
Figure 15   Schematic representation of nonlinear rheological model [67].

The model was calibrated with experimental data to obtain a set of parameters describing the material response at each strain rate. The calibration process was done using a MATLAB code of the 1-D version of MSU TP Ver. 1 and a curve fitting routine. The parameters were used for the material description of the liver sample in the development of a three-dimensional finite element model.

Using calibrated data from PSHPB experiments, several simulations at strain rates of 350, 550, 1000, and 1550 s^{-1} were performed (ABAQUS 6.9, [24]). Various stress components in the liver sample were analyzed and tracked throughout the compressive PSHPB procedure (Fig. 16).
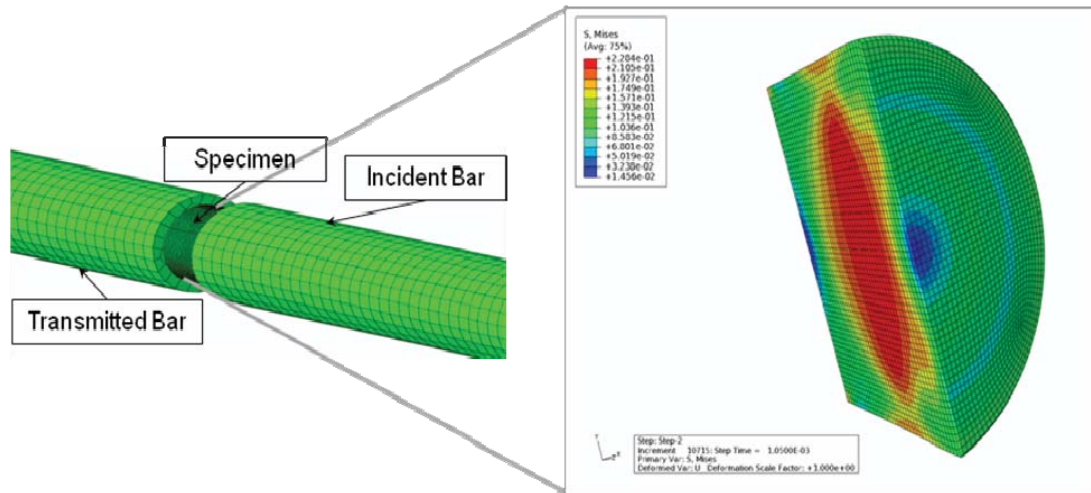
Figure 16   Color contours of von Mises stress from finite element simulations of polymeric split Hopkinson pressure bar. Enlarged portion shows a contour slice of σ_{Mises} in the specimen during a simulation at 550 s^{-1}.

The finite element model was composed of 22,010 linear hexahedral elements with the specimen containing 9200 elements. Mesh refinement was conducted to analyze the convergence of computational solutions. Boundary conditions included specified initial velocity for the striker bar , which allowed contacting the incident bar. The Finite Element Model exactly simulated the experimental PSHPB setup corresponding to different strain rates.

2.3 Results

PSHPB experiments show that liver tissue has a strain rate sensitive behavior under high rate compression (Fig. 17). Stresses were significantly higher as a strain rate increased from 350, 550, 1000, to 1550 s^{-1}.
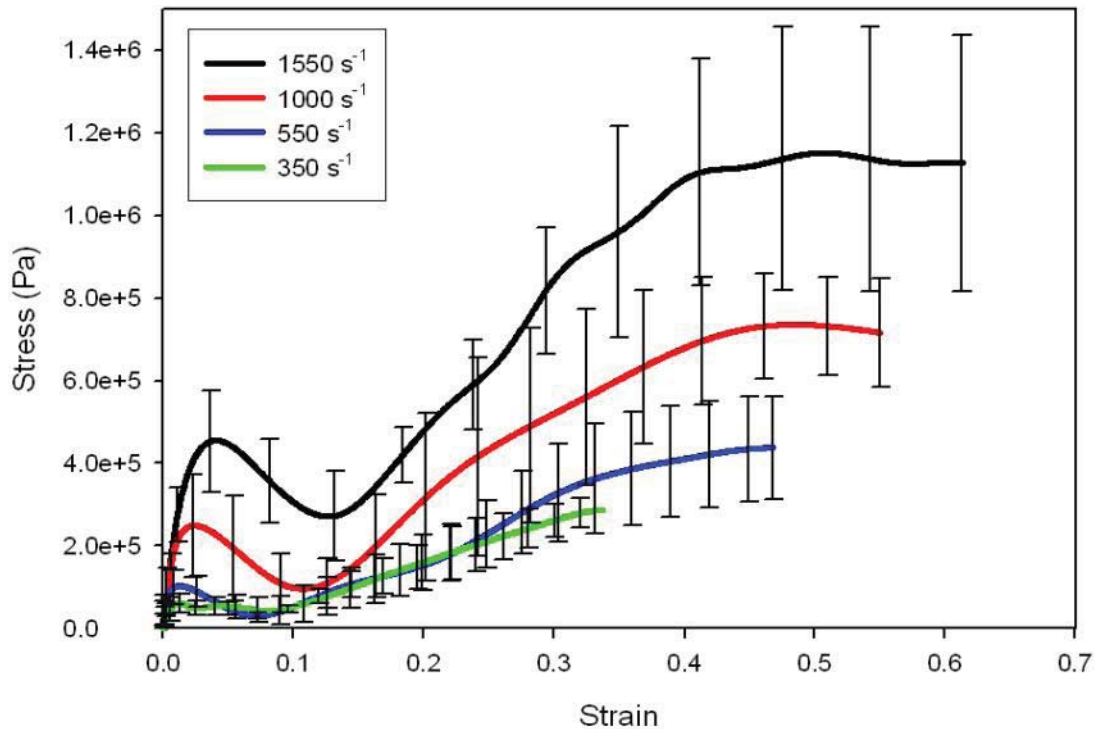
Figure 17   Stress-strain response of porcine liver tissue at 350, 550, 1000, and
1550 s^{-1} in Direction 1. n=4 for 350, 550, and 1000 s^{-1}; n=5 for 1550
s^{-1}. Error bars indicate standard deviation.

The resulting stress-strain behavior shows that the liver tissue exhibited an initial
stiffening behavior, followed by softening. After the softening, tissue hardening took
place until yielding and ultimate failure. The non-monotonic stress-strain behavior
described above was apparent for all four strain rates (350, 550, 1000, and 1550 s^{-1}).

To further examine the relationship between strain rate and material mechanical
response, data analysis of the stress-strain behavior at 350, 550, 1000, to 1550 s^{-1} was
performed by normalizing both the initial peak stress and the ultimate stress to valley
stress (lowest stress value following initial peak). Both the ratio of peak stress/valley

stress and the ratio of ultimate stress/valley stress decreased with the increase of strain rate (Table 1). Increasing strain rate from 550 to 1000 s^{-1} and from 1000 to 1550 s^{-1} yielded significant differences in the peak to valley stress ratios (ANOVA $p < 0.05$).

The stress-strain behavior of the liver tissues extracted from three orthogonal directions exhibited no significant difference at 350 s^{-1} (Fig. 18).

Table 1   Ratio of peak stress/valley stress and ratio of ultimate stress/valley stress shows an overall decreasing trend along with the increase of strain rate. (n=4)

Strain rate (s^{-1})	Mean Peak stress/Valley stress	Mean Ultimate stress/Valley stress
350	5.37 ± 4.59	21.92 ± 16.39
550	3.55 ± 1.56	13.36 ± 6.09
1000	3.00 ± 0.84	12.09 ± 3.56
1550	1.42 ± 0.24	12.48 ± 2.12
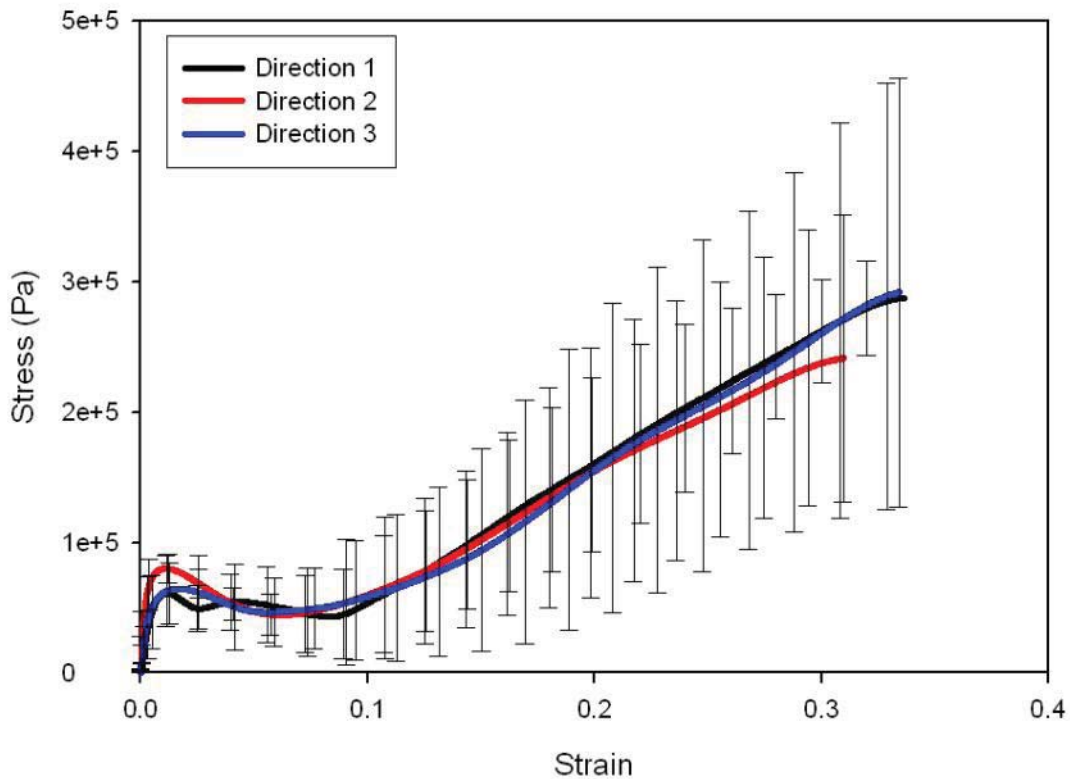
Figure 18   Mechanical stress-strain response of porcine liver tissue at 350 s^{-1} in Directions 1, 2, and 3 (n = 4) illustrating isotropy. Error bars indicate standard deviation.

The isotropic mechanical behavior was verified by the histological study, which revealed identical ultrastructure along the three orthogonal directions (Fig. 19, Table 2). The H&E staining showed black/purple cell nuclei and pink extracellular matrix of hepatocytes. Image analysis of the histological images revealed no differences regarding each of the three directions in terms of cell nuclear density, area fraction of cell nuclei, mean area of cell nuclei, and mean nnd. Overall, at high strain rates porcine liver tissue demonstrated a nonlinear, inelastic, strain-rate-sensitive mechanical response,

characterized by an initial peak and subsequent hardening until yielding and failure. Liver

tissue showed no directional dependency at high strain rates.
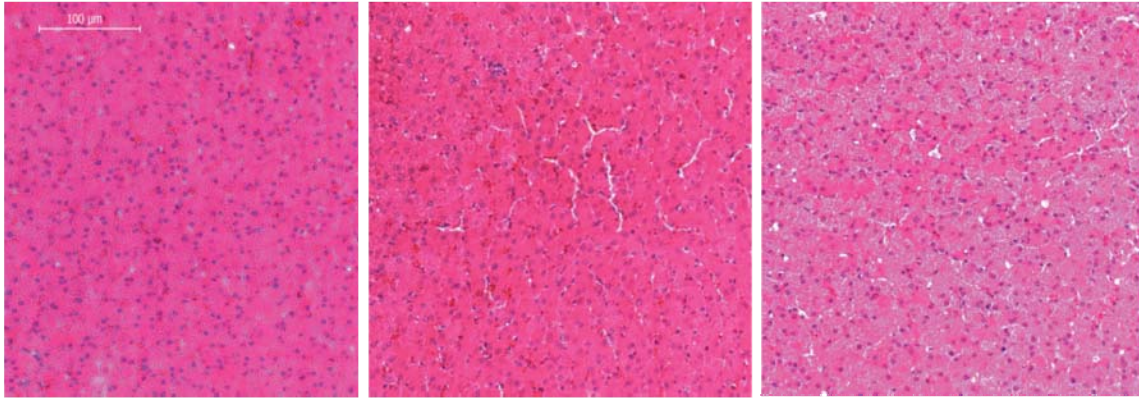
Figure 19   Liver histology revealing the tissue's homogeneity and isotropy. (a)
             Direction 1, (b) Direction 2, and (c) Direction 3. Liver tissues were
             fixed with 10% formalin at load-free condition.

Table 2   Image analysis results from Figure 8 (a), (b), and (c) revealing the
             tissue's homogeneity and isotropy.

	Direction 1	Direction 2	Direction 3
Objects	797	795	803
Cell nuclear density (/μm2)	4.08 x 10-3	5.91 x 10-3	4.11 x 10-3
Area fraction of cell nuclei	0.0979	0.0134	0.0806
Mean area of cell nuclei (μm2)	23.98 ± 15.58	22.6 ± 15.71	19.59 ± 7.73
Mean nnd (μm)	9.62 ± 3.14	8.44 ± 2.40	9.29 ± 3.12

The mechanical response of liver tissue was accurately captured by the MSU TP

material model (Fig. 20). Stress status in the cylindrical liver sample was revealed by

finite element modeling of the PSHPB test at a strain rate of 1000 s^{-1} (Fig. 21). The

contour plots of σ_{33} (axial stress) and σ_{Mises} were found to vary dramatically at the initial

stiffening, maximum stress of the peak, softening phase, valley stress, subsequent

hardening, and failure stress. The stress contours of the tissue sample also revealed a non-

uniform stress state throughout testing. The wave propagation observed via

computational modeling was consistent with the experimental results of the striker and

transmitted bars, thereby validating the testing procedure.
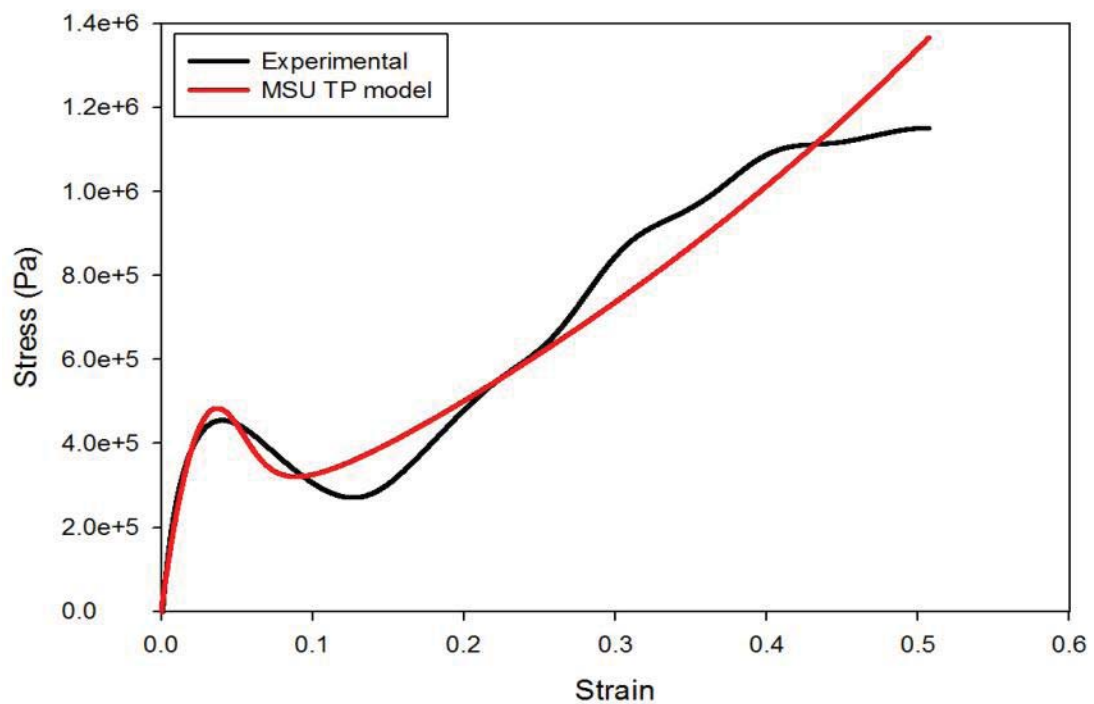
Figure 20   The MSU TP model shows a good fitting with the experimental data.
The theoretical curve and experiment data at 1550 s^{-1} were plotted as
a representation.
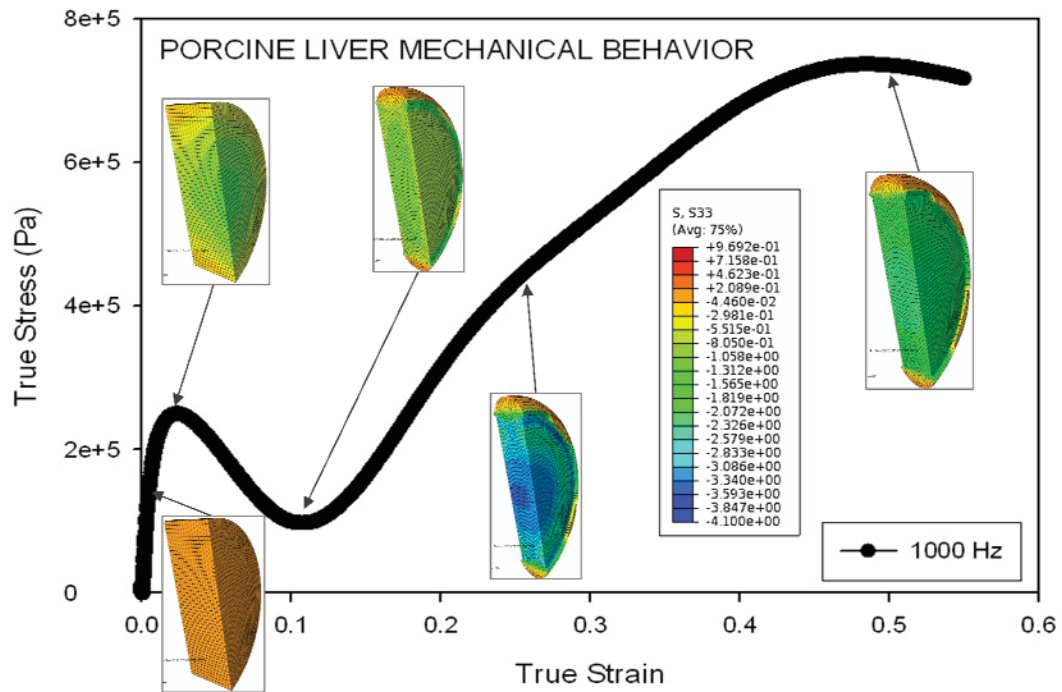
Figure 21   Finite element simulation results showing the contour plots of axial stress, σ_{33}, at various stages along true stress-true strain curve at 1000 s^{-1}.

2.4 Discussion

Hopkinson bar testing on soft tissues is relatively new; only a few studies have been reported most recently [51, 52, 68]. To obtain valid and accurate stress-strain data and further establish Hopkinson bar testing as the conventional high strain rate test for soft tissues, many variables were evaluated in this project. For example, the specimen aspect ratio was an important factor for consideration, so as to avoid unequal stress distribution in the sample and non-equilibrated input/output forces from an overly wide

sample. Van Sligtenhorst et al. suggested an optimal aspect ratio of approximately 2:1 for bovine muscle tissue samples to produce uniform stress distributions through the cross-section [52]. For choosing the appropriate aspect ratio, one must take into consideration two trends: (i) increasing the specimen aspect ratio can cause an increase in radial inertial effects; however, (ii) decreasing the specimen aspect ratio below a certain level could lead to non-uniform deformation along the longitudinal axis of the sample [52].

Van Sligtenhorst et al. and Song et al. showed the effects of specimen aspect ratio on the accuracy of PSHPB testing, and as a result, samples for the present study were prepared with the previously stated geometric criteria in mind. By generating consistent, repeatable data reflecting the intrinsic mechanical response of liver tissue, the optimal aspect ratio for liver tissue was determined to be 3:1.

The obtained true stress-true strain curves show a non-monotonic characteristic overall, similar to recently reported data from drop tower compression testing of human liver tissues at strain rates up to 62 s^{-1} [57]. Results from both studies indicate a loading path initiating with a sharp stiffening response, followed by softening, subsequent hardening, and then yielding until ultimate failure. It is notable that this initial stiffening does not appear in stress-strain plots obtained in the regime of low strain rates (< 10 s^{-1}), which often exhibit a monotonic, concave-upwards stress-strain relationship [65, 69]. Song et al. hypothesized that the stiffening was purely a result of inertia [51]; however, this may or may not be a complete conclusion. Similarly, Sparks et al. cited inertia as the main factor in initial stiffening but included dynamic changes in specimen geometry during loading as a factor in stiffening [57].

It is interesting to note that high strain rate testing of different tissues results in different degrees of initial stiffening. The results obtained by Prabhu et al. for brain tissue at high rate compression demonstrate a higher initial hardening peak when compared with liver data reported in this paper, and high rate compression of tendon tissue shows a minimum initial hardening peak (unpublished data). The above observation leads to a hypothesis correlating the initial stiffening with concentration of cellular content/water content. Specifically, tissues with higher cellular content have a higher initial stiffening peak than those of a more fibrous nature (e.g., brain > liver > tendon). One of the future aims of this research area is to better characterize various soft tissues to confirm the stiffening effect is actually an accurate representation of tissue behavior under high strain rate testing.

To our knowledge, no studies involving high strain rate Hopkinson pressure bar testing of porcine liver tissue exist. Moderate strain rate testing (20-62 s^{-1}) on human liver tissue was performed by Sparks et al., and showed similar trends in stress-strain plots, despite the difference in methodology, in which a drop tower technique was used on intact human livers [57]. Though these strain rates are considered as fairly high in the report, they are relatively low compared to the strain rates obtained in the present study. Through repetition of testing using the PSHPB apparatus, various input velocities of the striker bar resulted in consistent strain rates in the porcine liver tissue (Table 3).

Table 3   Correlation between striker bar speed and resultant strain rate of
             porcine liver tissue in high rate tests.

Velocity of striker bar (mph)	Strain rate of liver tissue (s^{-1})
6.487	350
9.843	550
13.645	1000
17.001	1550

Using the PSHPB method, striker bar speeds of approximately 6.5 - 17 mph corresponded to strain rates of 350 - 1550 s^{-1} in the liver tissue. For accurate replication of car crash scenarios, speed is a critical factor, and the impact speeds employed in the present study are more representative of speeds at which blunt trauma situations, such as those resulting from automobile accidents, occur.

The anisotropic mechanical response of liver tissue was also addressed in this study. The isotropy (or anisotropy) of liver tissue at high strain rates has not been defined or accepted in the present literature; therefore, evaluating this material property for modeling purposes was necessary. Experimental microstructural analysis and mechanical response data clearly showed that no difference exists among stress-strain behavior from testing along three orthogonal directions thus defining an isotropic medium. The histology results confirmed the microstructural similarities among Directions 1, 2, and 3. By analyzing the images via parameters involving cell nuclear area, cell count, and mean distance between neighboring cells, histology supports the multi-directional mechanical data, concluding that the liver tissue is isotropic.

2.5 Conclusion

The use of a PSHPB apparatus for high strain rate testing of porcine liver tissue reveals the inelasticity, isotropy, and strain rate sensitivity of the liver tissue. In conclusion, (i) the liver tissue response at high rate compression is characterized by an initial hardening peak, followed by softening, and then by strain hardening to failure; (ii) the liver mechanical stress-strain behavior increased as the applied strain rate increased; and (iii) isotropic high rate material behavior was observed along three orthogonal directions and confirmed by liver histological microstructure.

In addition to these three conclusions, some other important points are worth mentioning. The wave propagation predicted by the finite element PSHPB simulation was consistent with the experimental results, thus substantiating the present results of the PSHPB. However, the computational simulation of the PSHPB process also shows that a uniform stress state was not fully achieved in the cylindrical sample. This limitation implies that future work is warranted to perfect the PSHPB technique in soft tissue high rate characterization.

This novel approach using polymeric bars for high rate impact of porcine liver tissue serves as a benchmark for future high strain rate testing of soft tissues. The experimental data coupled with the finite element model can be implemented in large-scale computational models of the human body for simulation of high strain rate scenarios such as automobile accidents for validating the efficacy of various safety features.

2.6 Discussion and Future Study

One of the specific aims of this research is to establish a methodology for high strain rate testing of soft tissues. Although we feel we have made much progress in the field, there are still some important issues that need further investigation on in order to establish a stable methodology.

One question is whether or not the inertia effect present in high strain rate testing a product of the testing conditions or the material itself. The initial stiffening at the beginning of the stress strain curve merits some thorough analysis. It has been hypothesized by Van Sligtenhorst that the "bump" is the effect of inertia effect and not the material [52]. Other researchers, Clemmer et. al, hypothesized that it is in fact the effect of the water in the material that causes the initial stiffening. They evaluated lyophilized samples and showed that the initial "bump" disappeared. These studies show that there is some discrepancy on the analysis of tests.

Other issues include the data analysis assumptions of the David viscoelastic software. The software assumes that the test is a 1-D test and considers stresses in the axial directions to be negligible. In metals, FE validations confirm that this assumption is valid, but for soft tissue, this area may be of concern. Regarding the viscoelastic response of soft tissue, it may be that this 1-D assumption cannot be made; therefore, preventing an accurate analysis of material properties.

Considering that research is in its nature dynamic and collaborative, many more studies need to done in order to come to a conclusion concerning the aforementioned issues. In this study, we proposed a new methodology in Split Hopkinson bar, with aspect ratio considerations in hopes of producing accurate high strain biomechanical data

47

of the liver. With continuing efforts in conducting research in this direction, we hope to

address these issues and present an accepted methodology for high strain rate

biomechanics of soft tissues.

CHAPTER III

QUANTITATIVE ANALYSIS OF DAMAGE EVOLUTION IN PORCINE LIVER VIA

INTERRUPTION TESTING APPROACH

3.1 Introduction

A computational model capable of assessing traumatic injury is of increasing

interest and is currently a growing area of research. With increasing requirements for

automobile safety, computational models capable of including the true structure-property

relationships of tissues and thus simulating organ deformation and injury during high

impact scenarios would be extremely valuable for optimizing safety measures. Previous

evaluations of automobile safety considered the effects of concentrated stresses on

dummies, cadavers, and animals during various accident events. However, an objective

understanding of injury mechanisms and proper threshold forces were not thoroughly

discussed [70, 71]. For example, Baker et.al reported an automobile accident in which the

seat belt caused a rupture of the stomach leading to the death of the victim.[72] This

shows the potential injuries that can be caused by current safety devices as well as their

limitations. Improved understanding of injury mechanism will produce safety devices

that are better equipped to prevent injury.

Much effort has been directed towards FE models that simulate traumatic injury

with the primary focus of future development of safety devices [73-81]. However, little

effort has been directed towards understanding the failure mechanisms of various organs during and after impact, especially within the abdominal region. Liying et. al and Newman et al. performed evaluations on proposed a mechanism for understanding a threshold value for traumatic brain injury [70, 71]. Newman et al also investigated mild head trauma by utilizing dummies [71]. Further studies must be conducted to gain a better understanding of where injury occurs in order to determine a threshold criterion that will make these FE models much more meaningful.

As discussed earlier, abdominal organs are very susceptible to injury in automobile accidents, the liver being the most vulnerable abdominal organ [34]. There have been a few studies investigating the characterization of the liver for robot assisted surgeries, for *in vivo* biomechanical testing approaches, and for general characterizations [82-88]. In this study, we propose an interruption testing approach, which will provide greater insight into the behavior and progression of damage in the liver. By evaluating histological images at various strain levels with image analyzing software (CAVS Image Analyzer), we are able to quantitatively determine a trend describing the damage evolution of the sample. The data gathered from this study can be used for development and formulation of constitutive models, which are then used to create damage models valuable for FE simulations.

3.1.1 Extracellular Matrix of Liver

In the field of failure mechanics, a detailed understanding of the structure of the material of interest is important to come to conclusions and determine methods to prevent

failure. Similarly, an investigation in the structure and load bearing nature of the liver is important for our understanding of the damage evolution.

The main load bearing element of soft tissues in the body is the extracellular matrix (ECM) [63, 89]. The ECM is a complex macromolecular structural network that lies between the interfaces of cells and various membranes. It is responsible for the structural integrity of many organs/tissues and also contributes to many physiological events by modulating processes that include: cell attachment, migration, differentiation, repair, and development. ECM is readily synthesized by various cells depending on the organ/tissue and is also maintained by the cellular environment. Generally, extracellular matrix is composed of different types of collagen, elastin, structural glycoproteins, and proteoglycans [89]. In different organs and tissues in the body, there will be a different concentration and composition of the components of ECM. This allows for different and unique organ/tissue properties that are tailored to each organ/tissue's individual needs.

3.1.1.1 Collagen

Collagen is the most abundant protein in the human body. Currently, there are 24 known types of collagen comprised from more than thirty genes. These types of collagen differ by degree of glycosylation and chain composition. The collagen hierarchy can be broken down from its highest form as a fiber, to a fibril, to a molecule, to an amino acid chain. The amino acid chain is composed of the sequence Gly-X-Y repeats with X and Y representing most often proline and hydroxyproline respectively [63, 89]. The individual alpha chains form left-handed helices and contain approximately three residues per turn. In order to form the collagen molecule, three of the amino acid chains, termed alpha

chains, coil around each other in a right-handed fashion. Collagen molecules are about

300 nm long and 1.4 nm in diameter. These collagen molecules are oriented in a quarter-

staggered pattern which is shown in Figure 22.
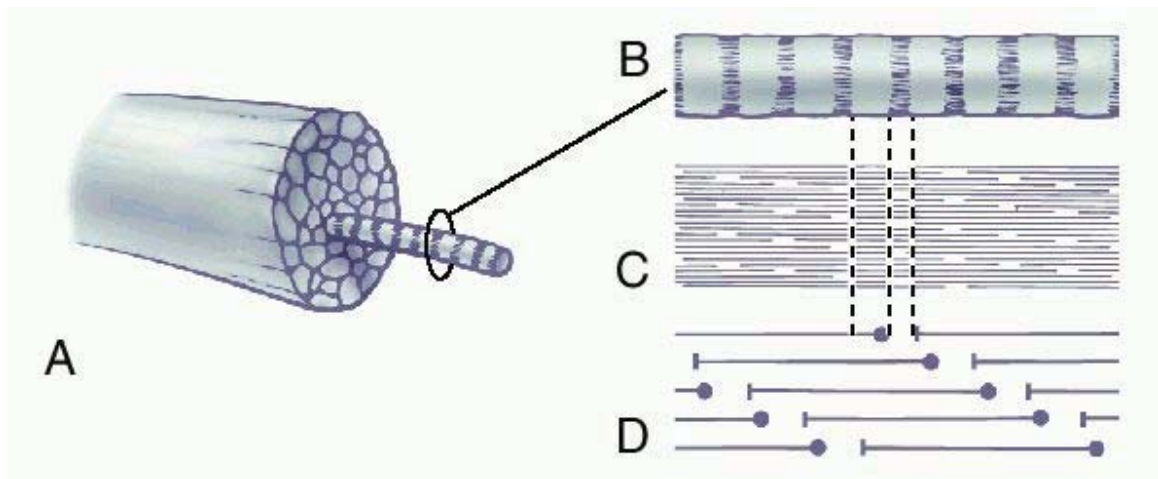
Figure 22   Collagen fibril showing the quarter-staggered pattern, (a) Fibril, (b) D
period, (c,d) quarter-staggered pattern; (Merck Source)

Finally, the combined aligned fibrils, bonded by small proteoglycan links, form a

collagen fiber. The amount and alignment of collagen differs from tissue to tissue. In

tendons and ligaments, there is a high density of aligned collagen. This makes sense

because of the function of tendons and ligaments in the body as tensile load bearing

tissues. Other tissues such as blood vessels contain a more balanced mix of collagen and

other ECM components in order to compensate for the intrinsic expanding and pulsing

aspects of blood vessels. Non load bearing organs therefore are composed of another

distribution of ECM components. Their collagen orientation can be described as a disordered network of collagen fibers immersed in a mix of proteins and proteoglycans.

Collagen serves an important function in the human body especially as an ECM constituent. It is the main load bearing constituent in virtually all soft tissues. Y. C. Fung compared collagen to steel in our society [63]. Steel is found in many structures such as bridges, vehicles, buildings, utensils, and instruments; similarly, collagen is found in our blood vessels, skin, tendons, bone, etc. and is essential for their mechanical integrity. It has been shown that the strength of a material, its failure strength or ultimate stress, is governed by the collagen; however, another component that contributes greatly to a soft tissue's mechanical response is elastin.

3.1.1.2 Elastin

As collagen provides the strength of a soft tissue, elastin provides the elasticity [90]. Elastin is a protein found in large proportions in the walls of arteries and veins, and the lungs. It presents itself as thin strands and when pulled in tension, shows an almost linear curve with a small hysteresis area. In horses and calves, the ligamentum nuchae is almost purely elastin. It is found along the top neck of horses and calves and allows them to keep their head up without expending a large amount of energy.

The elastin molecule is produced from its precursor molecule tropelastin. It has been shown that tropoelastin is synthesized intracellular and cross-linked extracellularly to form elastin. The mature elastin is inert and so stable that in the normal body environment, it lasts throughout a whole lifetime.

3.1.1.3 Glycoproteins

In extracellular matrix, glycoproteins play a major role in cell adhesion processes. They are proteins that contain oligosaccharide chains and are covalently attached to polypeptide side chains. In many cases, glycoproteins will interact with specific amino acid sequences at cellular receptor integrins allowing for cell attachment. Examples of glycoproteins include laminin, enactin, fibronectin, and tenascin.

3.1.1.4 Proteoglycans

Proteoglycans are glycoproteins that contain a large amount of glycosaminoglycan (GAG) side chains which are covalently connected to a core protein. In cartilage, proteoglycan aggregates aid in allowing cartilage to undergo repetitive compressive stresses; however, in many cases it is unclear whether or not proteoglycans are involved in the mechanical integrity of the ECM. It is known that proteoglycans are involved in the regulation of molecule movement as well as the activity of proteins and signaling molecules.

3.1.2 Liver ECM

Liver ECM is composed of five types of collagen: collagen type I, collagen type III, collagen type V, collagen type VI, and collage type VII [91]. It also contains the glycoproteins fibronectin, and tenascin. Hepatic ECM in the liver capsule, major septa, and portal spaces are analogous to those of other glandular organs.   In the liver, ECM is synthesized by mainly three cell types: hepatocytes, endothelial cells, and Ito cells. Hepatocytes have been shown to contain the mRNA for collagen type I; endothelial cells

have been shown to synthesize the ECM components collagen type I, III, IV, and laminin antigens; and Ito cells have been demonstrated to synthesize many ECM components *in vitro*. Studies concerning hepatic ECM have investigated the physiological processes that interact with the ECM; however, there is not a clear understanding of how it bears load. Because the liver is not a load bearing organ, the ECM is not tailored to withstand repetitive loads or high stresses. However, there is a structural and mechanical integrity provided by the ECM, and therefore the hepatic ECM is of great interest in analyzing the progression of damage with increasing strain.

3.2 Methods

Porcine livers from healthy pigs (6-month old) were obtained from a local abattoir. The specimens were stored in phosphate buffered saline (PBS) at 4°C soon after extraction and transported to the laboratory. All testing was performed within 12 hours of extraction. Samples were cut into various sizes depending on the testing mode (compression, tension, shear). Samples were obtained from various lobes after concluding that there was no significant difference in the biomechanical data varying from lobe to lobe. Compression samples were extracted using an 8 mm diameter biopsy punch and cut into lengths of 5 mm. Tension samples were cut into dogbone shapes of 10 mm in length, 2 mm in width, and 1 mm thick. Shear samples were cut into squares of 10 mm by 10 mm.

3.2.1 Biomechanical Testing

Biomechanical testing was conducted using the Mach-1 Micro Mechanical Tester using a 1 kg load cell. The Mach-1 system consists of a variety of functions with many flexible parameters that allows users to generate programs for any desired test. In this study, quasi-static biomechanical characterization of the liver, and interruption biomechanical tests were completed. Also, in order to determine proper strain levels for interruption testing, failure tests were performed and stress strain curves were analyzed to determine strain levels that would thoroughly describe the progression of damage until failure.

3.2.1.1 Tension
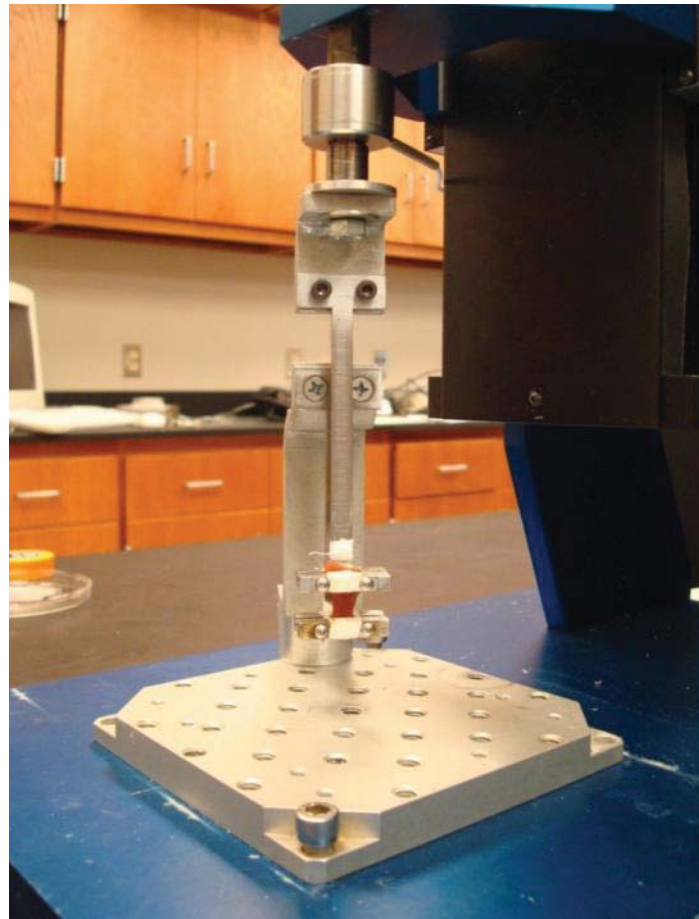
Figure 23   Experimental set up for tensile testing of porcine liver

Tension samples were cut into dogbone shapes of 10 mm in length, 2 mm in width, and 1 mm in thickness. Tension samples were clamped using custom made grips and pulled to strains of 10%, 20%, 30%, and failure (Figure 23). A preload of 0.5 grams was set for the test and the displacement rate was set at 10 mm/min. Each sample was preconditioned 10 cycles before being pulled to a certain strain level or failure. For interruption testing, samples were submerged in 10% neutral buffered formalin

immediately after testing was completed. A simple plastic bag was placed around the specimen and filled with 10% neutral buffered formalin. Samples were kept submerged for three hours and then placed in a container with fresh formalin and stored in the 5 deg C refrigerator. Samples were fixed in formalin for at least 72 hours before histological analysis.

3.2.1.2 Compression
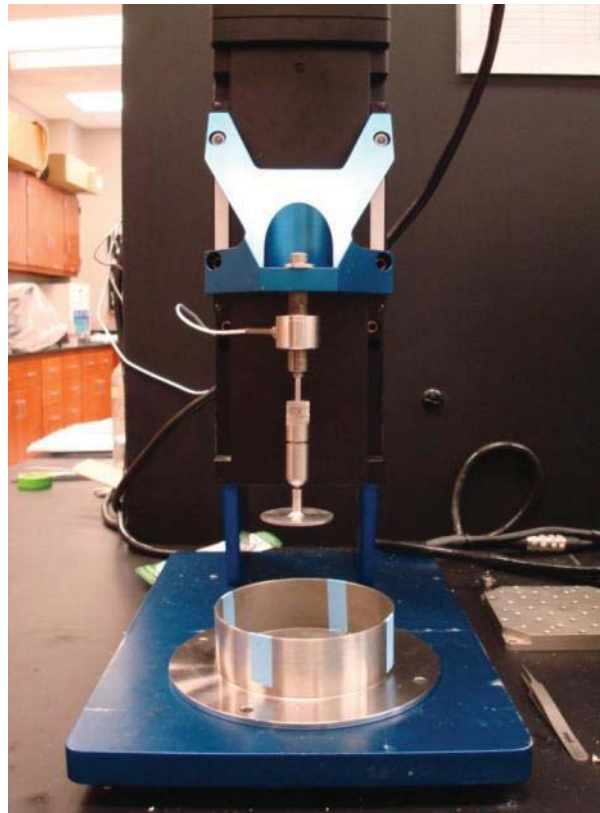
Figure 24   Experimental set up for compression testing of porcine liver

Compression samples were cut out using an 8 mm biopsy punch. Samples were 8 mm in diameter and 5 mm in height. The compression apparatus consists of a platen and a base with cylindrical walls (Figure 24). Samples were glued with cyanoacrylate between the base and the platen before testing began. For the precise measurement of height, the platen was used in conjunction with the Mach-1 software. By moving the platen to the bottom of the base and zeroing the position, we were able to use the find contact function and determine the height of each sample in microns. Each sample was

preconditioned for ten cycles and then compressed to its prescribed strain level. Similar to the tension samples, immediately after the testing was complete, 10% neutral buffered formalin was poured into the base to completely submerge the sample. The sample was left in the base for three hours before removal. The samples were then transported into a container with fresh formalin and placed in a 5ºC refrigerator.

3.2.1.3 Shear
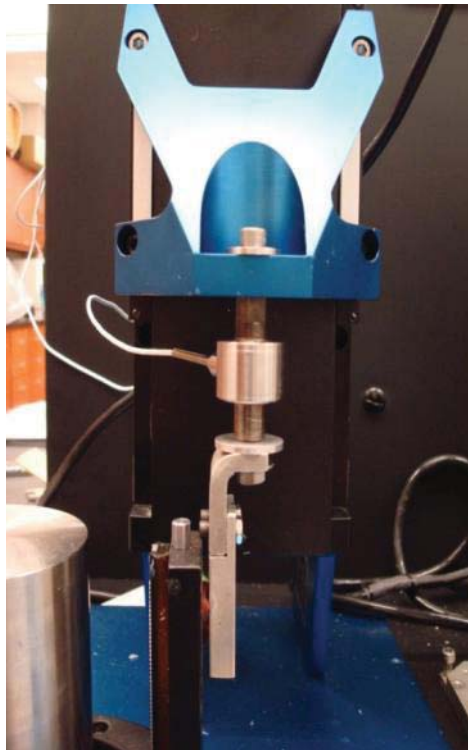
Figure 25   Experimental set up for shear testing of porcine liver

Shear samples were cut out using scalpels to the dimensions of 10 mm by 10 mm. A custom made shear device that included a polycarbonate container was incorporated

into the Mach-I (Figure 25). The purpose of the polycarbonate container was to allow for formalin fixation of the samples after testing. The testing apparatus consisted of two plates, one stationary and one mobile. The samples were glued using cyanoacrylate onto the stationary plate first and then glued to the mobile plate before testing. Unlike the tension and compression tests, the shear test was a load dependent test. Therefore, the functions used for the program were significantly different. Samples were preconditioned for 10 cycles and then fixed in formalin immediately after testing. Similar to the other testing types, the sample was submerged for at least three hours before being moved into a 5ºC refrigerator. Stress strain curves for shear testing were generated as stress vs shear angle graphs. Referring to Figure 26, the deformation, shear angle, can be calculated by taking the arctangent of the change in displacement (y) over the thickness (x).
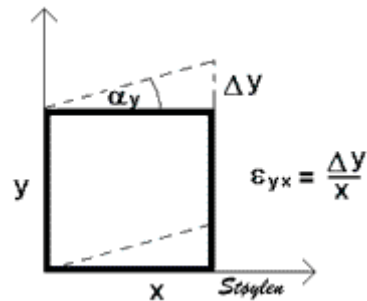
Figure 26   Example of conventional shear angle diagram; From (NTNU)

3.2.2 Histological Staining

After being submerged for at least three days, liver samples were removed from 10% neutral buffered formalin, they were dehydrated in a graded ethanol series. Tension, compression and shear samples were then embedded in Paraplast with CitriSolve as a transitional fluid, sectioned to a thickness of 7 μm, and subjected to Hematoxylin & Eosin (H&E) staining. In H&E staining, liver cell nuclei were stained black/purple and extracellular matrix proteins pink. H&E staining was utilized to show tissue microstructure at various strains.

Liver samples for each testing mode were sectioned at the cross section of each sample. Three samples for each strain level was evaluated using histology.

3.2.3 Image Analysis

ImageAnalyzer v.2.2-0 software (CAVS, Mississippi State University) was used for microstructural analysis of histological images from each sample at various strain levels. The parameters obtained for each image during analysis included the following: Number Density, Area Fraction, Mean Area, Mean Nearest Neighbor Distance. The histology showed distinct voids that progressed and increased in size as strain increased. ImageAnalyzer was utilized to track all the voids and quantify them using the above parameters. Number density represents the total number of voids relative to the area of an image; Area fraction represents the ratio of the total void area to the total image area; Mean area represents the average area of the voids; and mean nearest neighbor distance represents the distance between neighboring voids.

Three samples from each strain level were evaluated using image analysis. Within each histological image, three images were taken at three locations and analyzed using Image Analyzer. This allowed for a balanced analysis of the histological images. A total of nine samples were analyzed in tension; a total of twelve samples were analyzed in compression; and a total of nine samples were analyzed in shear.

3.3 Results

Conventional biomechanical tests were completed for the liver in three testing modes: tension, compression, and shear (Figure 26; Figure 27; Figure 28). Tension samples were pulled to 20% strain and had stress values of about 20.5 kPa. Compression samples were pushed to strains of about 40% and generated stress values of 36.3 kPa. Shear samples were sheared using a load dependent protocol to a stress value of 1.5 kPa. Representative stress strain curves were assembled for each testing mode. Failure tests were also evaluated for tension and shear. Shear samples failed at stresses of 5.24 kPa, and tensile samples failed at an ultimate stress of 8.8 MPa.
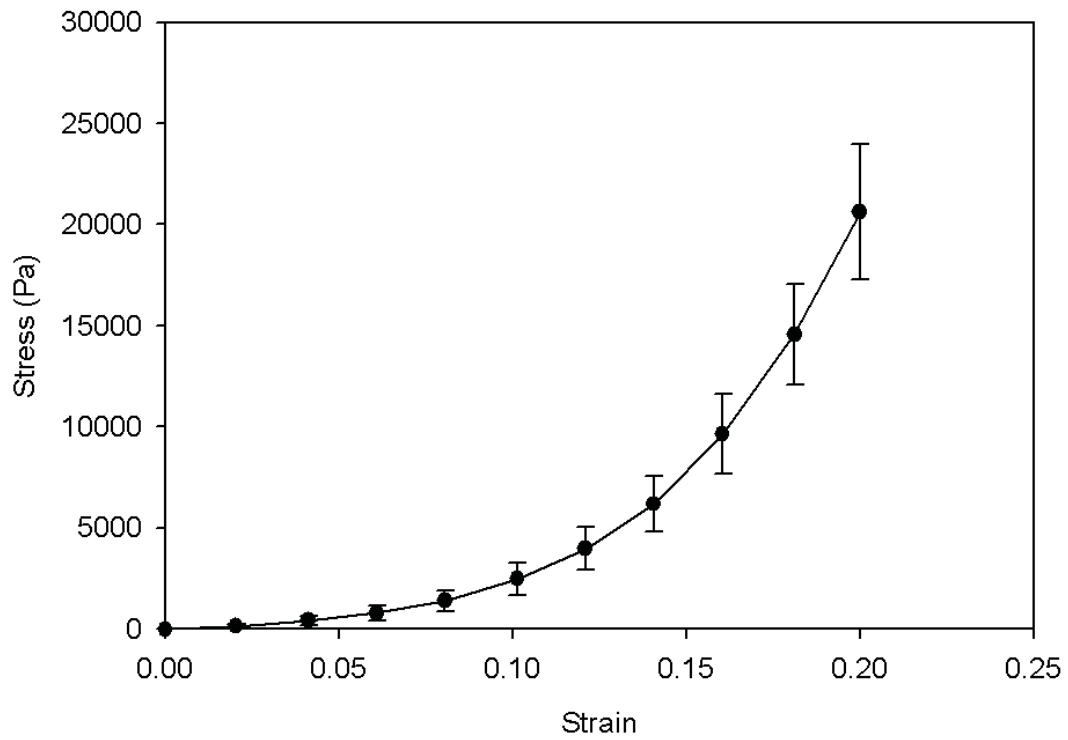
Figure 27   Representative stress strain curves for tensile testing of porcine liver
to 20% strain
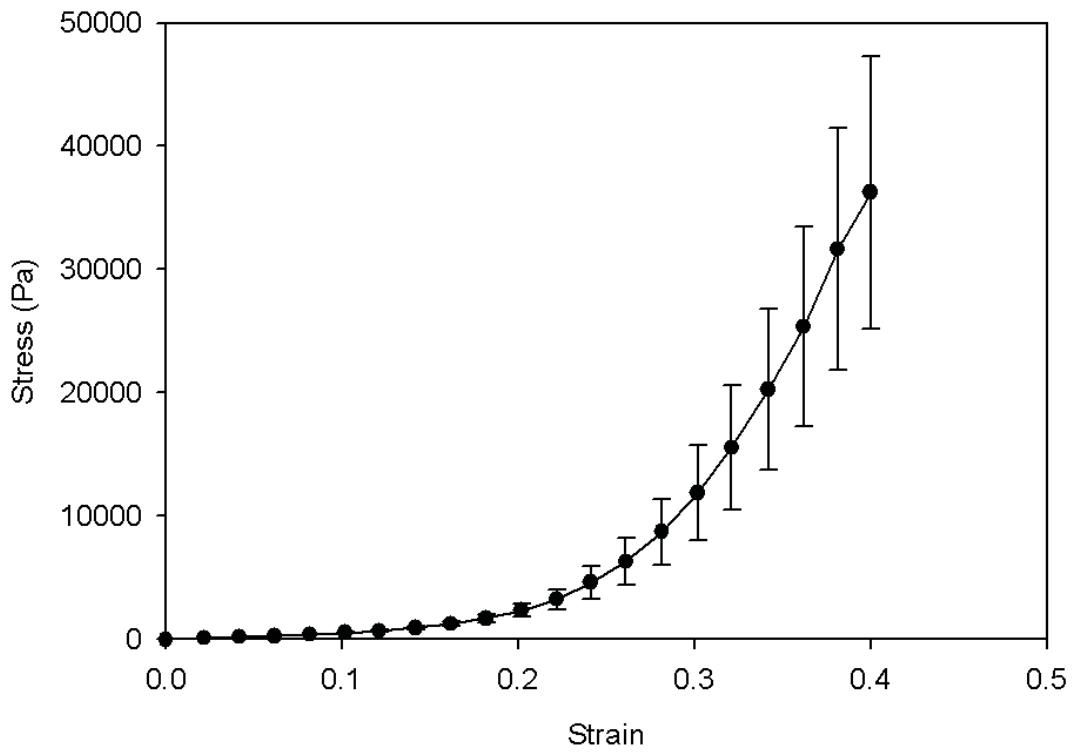
Figure 28   Representative stress strain curve of compression testing of porcine liver to 40% strain
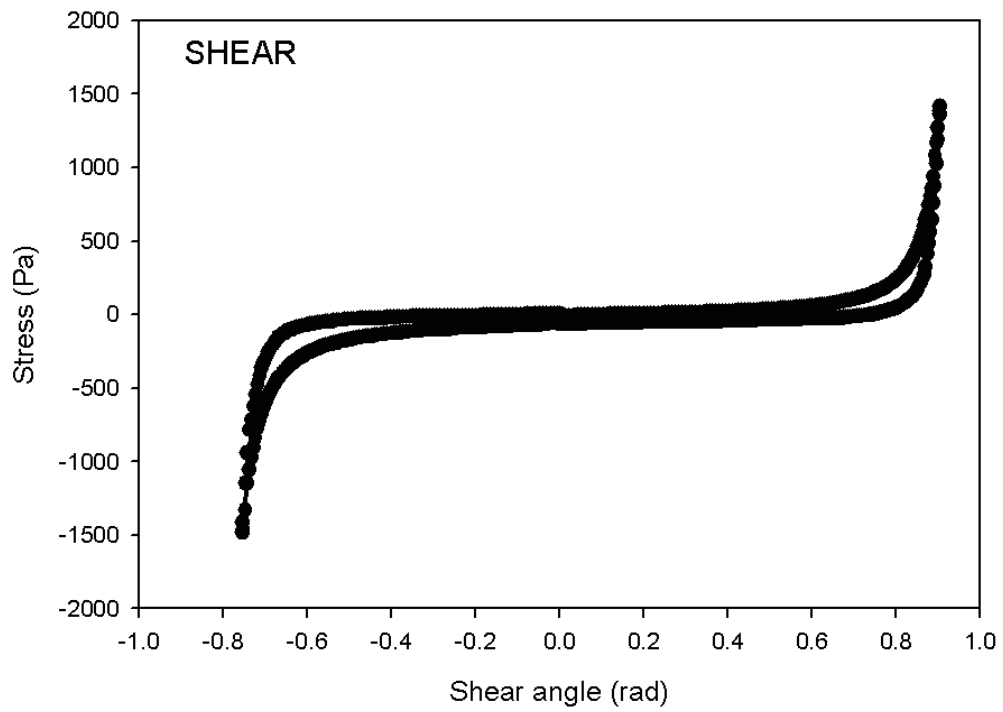
Figure 29   Representative stress strain curve of shear testing of porcine liver to a
load of 1500 Pa.

Figure 30   Representative histological images of damage evolution of porcine liver via tensile interruption testing at (a) Control, (b) 10%, (c) 20%, and (d) 30% strain

Table 4   ImageAnalyzer parameters for damage evolution of tensile tests at Control, 10%, 20%, and 30% strain

	Object	No. Density (/μm^2)	Area Fraction	Mean area (μm^2)	Mean nnd (μm)
Control	18.33 ± 15.50	$2.30 \times 10^{-5} \pm 1.95 \times 10^{-5}$	0.00142 ± 0.0014	30.061 ± 20.989	100.38 ± 69.49
10%	105.78 ± 34.69	$1.32 \times 10^{-4} \pm 4.35 \times 10^{-5}$	0.00624 ± 0.002	50.64 ± 9.71	44.039 ± 8.56
20%	139.44 ± 58.64	$1.75 \times 10^{-4} \pm 7.36 \times 10^{-5}$	0.0117 ± 0.0046	68.99 ± 20.2	36.632 ± 5.35
30%	$141 + 50.57$	$3.82 \times 10^{-4} + 6.3 \times 10^{-4}$	$0.0161 + 0.00595$	$126.37 + 106.04$	$36.805 + 7.325$

Quantitative parameters from each sample showed distinctive trends. For the three tension strain groups (10%, 20%, 30%), the object count, number density, area fraction, and mean area all increased with each group/increasing strain. Object count generated values of 105.78 ± 34.69 for 10% strain, 139.44 ± 58.64 for 20% strain, and 141 ± 50.57; Number density generated values of $1.32 \times 10^{-4} \pm 4.35 \times 10^{-5}$ /μm^2 for 10% strain, $1.75 \times 10^{-4} \pm 7.36 \times 10^{-5}$ /μm^2 for 20% strain, and $3.82 \times 10^{-4} \pm 6.3 \times 10^{-4}$ /μm^2 for 30% strain; Area Fraction generated values of 0.00624 ± 0.002 for 10% strain, 0.0117 ± 0.0046 for 20% strain, and 0.0161 ± 0.00595 for 30% strain; and Mean Area generated values of 50.64 ± 9.71 μm^2 for 10% strain, 68.99 ± 20.2 μm^2 for 20% strain, and 126.37 ± 106.04 μm^2 for 30% strain. Mean Nearest Neighbor Distance (nnd), however, showed a declining trend. Mean nnd generated values of 44.039 ± 8.56 μm for 10% strain, 36.632 ± 5.35 μm for 20% strain, and 36.805 ± 7.325 μm for 30% strain.

Figure 31   Representative histological images of damage evolution of porcine liver via compression interruption testing at (a) Control, (b) 10%, (c) 20%, (d) 30% strain, and (e) 40% strain

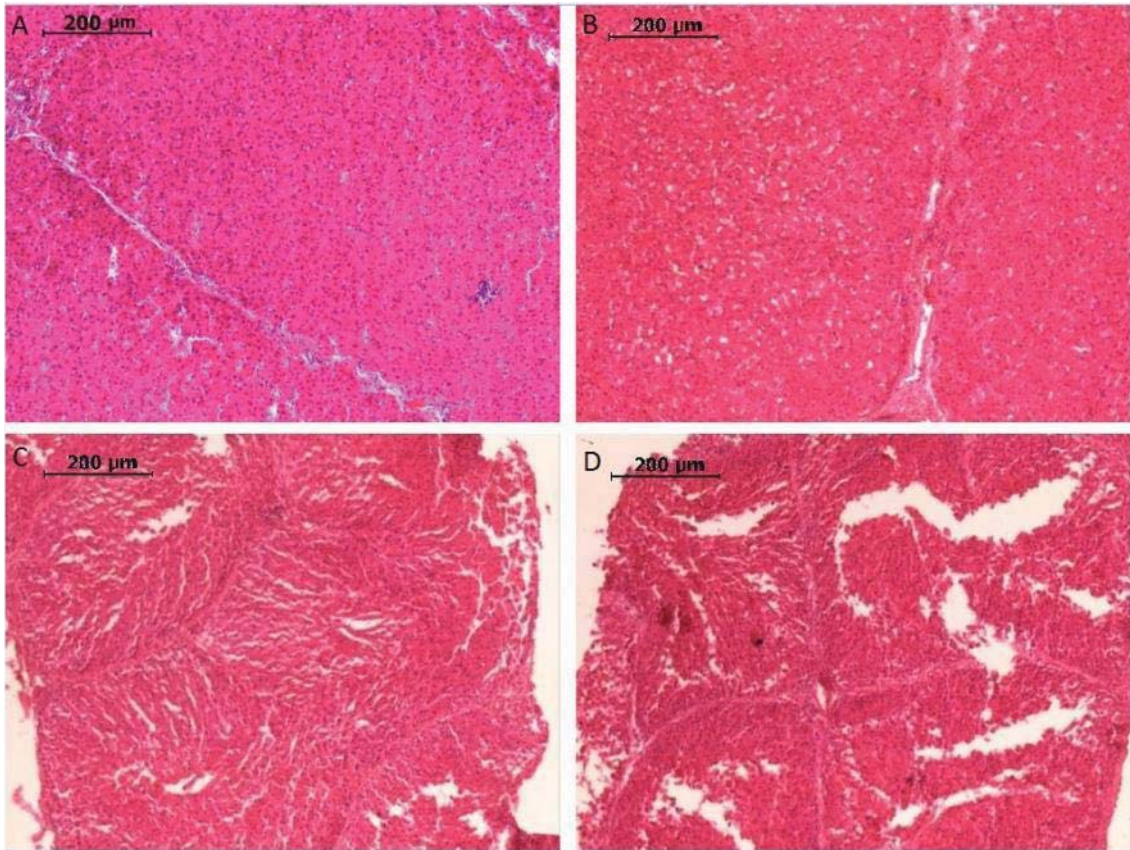Table 5   ImageAnalyzer parameters for damage evolution of compression tests at Control, 10%, 20%, 30%, and 40% strain

	Object	No. Density (/μm^2)	Area Fraction	Mean area (μm^2)	Mean nnd (μm)
Control	18.33 ± 15.50	$2.30 \times 10^{-5} \pm 1.95 \times 10^{-5}$	0.00142 ± 0.0014	30.061 ± 20.989	100.38 ± 69.49
10%	52.16 ± 27.3	$6.54 \times 10^{-5} \pm 3.42 \times 10^{-5}$	0.00327 ± 0.0018	49.12 ± 6.32	62.797 ± 21.61
20%	81.2 ± 33.4	$1.01 \times 10^{-4} \pm 4.20 \times 10^{-5}$	0.00607 ± 0.00251	61.55 ± 24.55	49.129 ± 9.68
30%	223.6 ± 101.96	$2.81 \times 10^{-4} \pm 1.27 \times 10^{-4}$	0.0176 ± 0.00913	60.77 ± 9.025	32.978 ± 6.473
40%	275 ± 131.67	$3.45 \times 10^{-4} \pm 1.65 \times 10^{-4}$	0.025 ± 0.0131	71.88 ± 6.188	29.642 ± 6.23

For the four compression strain groups (10%, 20%, 30%, 40%), the object count, number density, area fraction, and mean area all increased with increasing strain similar

to the tension groups. Object count generated values of 18.33 $\pm$ 15.50 for Control, 52.16 $\pm$ 27.3 for 10% strain, 81.2 $\pm$ 33.4 for 20% strain, 223.6 $\pm$ 101.96 for 30% strain, and 275 $\pm$ 131.67 for 40% strain. Number Density generated values of 2.30 X 10^{-5} $\pm$ 1.95 X 10^{-5} / μm^2 for Control, 6.54 X 10^{-5} $\pm$ 3.42 X 10^{-5} /μm^2 for 10% strain, 1.01 X 10^{-4} $\pm$ 4.20 X 10^{-5} /μm^2 for 20% strain, 2.81 X 10^{-4} $\pm$ 1.27 X 10^{-4} /μm^2 for 30% strain, and 3.45 X 10^{-4} $\pm$ 1.65 X 10^{-4} /μm^2 for 40% strain. Area Fraction generated values of 0.001423 $\pm$ .0014 μm^2 for Control, 0.00327 $\pm$ 0.0018 μm^2 for 10% strain, 0.00607 $\pm$ 0.00251 μm^2 for 20% strain, 0.0176 $\pm$ 0.00913 μm^2 for 30% strain, and 0.025 $\pm$ 0.0131 μm^2 for 40% strain. Mean Area generated values of 30.061 $\pm$ 20.98 μm for Control, 49.12 $\pm$ 6.32 μm for 10% strain, 61.55 $\pm$ 24.55 μm for 20% strain, 60.77 $\pm$ 9.025 μm for 30% strain, and 71.88 $\pm$ 6.188 μm for 40%. Mean nnd, similar to tension, showed a declining trend. Mean nnd generated values of 100.381 $\pm$ 69.49 for Control, 61.797 $\pm$ 21.61 for 10% strain, 49.129 $\pm$ 9.68 for 20% strain, 32.978 $\pm$ 6.473 for 30% strain, and 29.642 $\pm$ 6.23 for 40% strain.
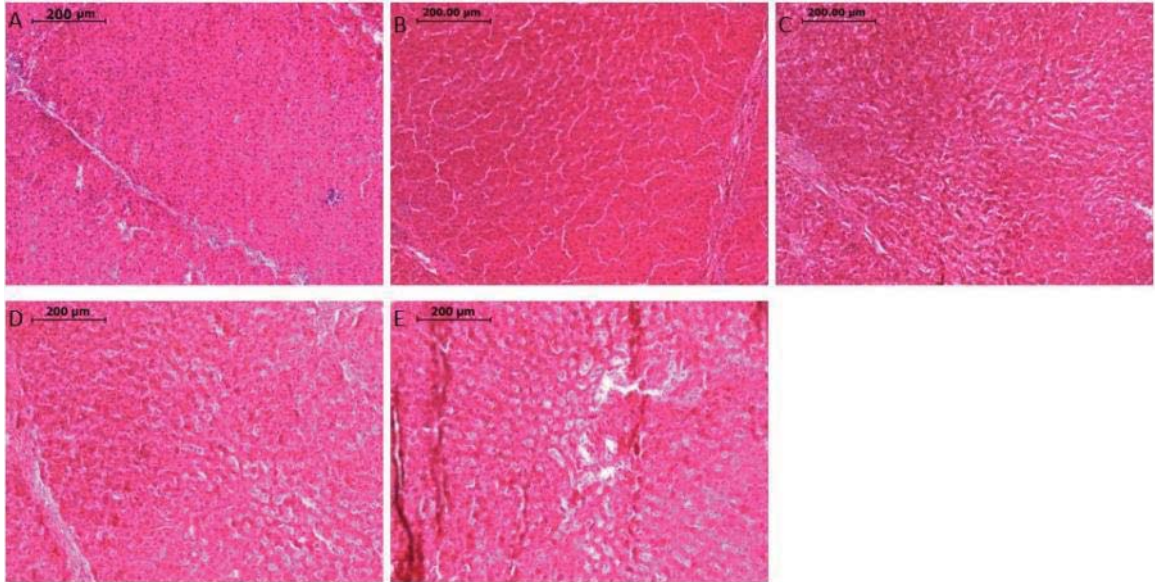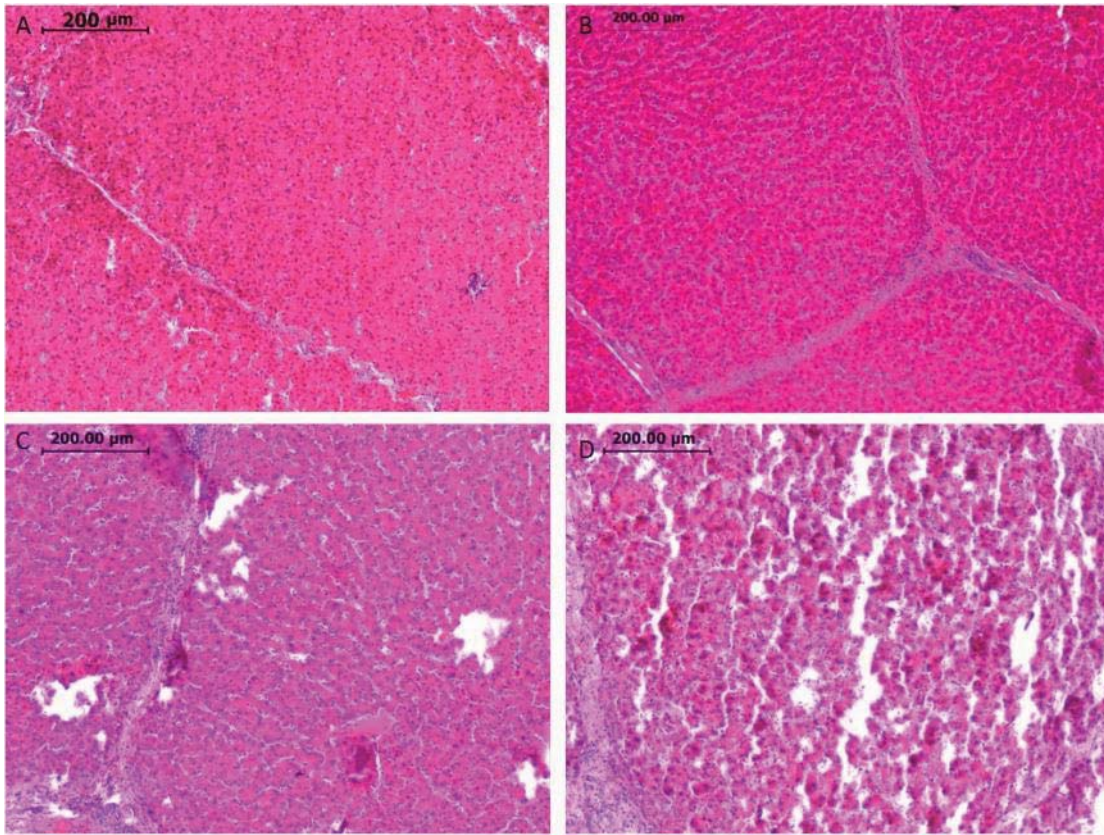
Figure 32   Representative histological images of damage evolution of porcine liver via shear interruption testing at a shear angle of (a) Control, (b) 0.8, (c) 0.9, and (d) 1.0 radians.

Table 6   ImageAnalyzer parameters for damage evolution of shear tests at a shear angle of Control, 0.8, 0.9, and 1.0 radians.

	Object	No. Density (/μm^2)	Area Fraction	Mean area (μm^2)	Mean nnd (μm)
Control	18.33 ± 15.50	$2.30 \times 10^{-5} \pm 1.95 \times 10^{-5}$	0.00142 ± 0.0014	30.061 ± 20.989	100.38 ± 69.49
0.80 rad	49.11 ± 31.99	$1.59 \times 10^{-4} \pm 3.09 \times 10^{-4}$	0.00275 ± 0.002	42.135 ± 7.624	79.91 ± 41.354
0.90 rad	124.22 ± 82.04	$4.96 \times 10^{-4} \pm 1.09 \times 10^{-4}$	0.00839 ± 0.0064	49.024 ± 9.72	44.94 ± 20.11
1.0 rad	160.22 ± 37.82	$6.03 \times 10^{-4} \pm 8.34 \times 10^{-4}$	0.0120 ± 0.0048	58.638 ± 12.33	36.26 ± 3.20

Finally, for the shear group of strain angles 0.8 radians, 0.9 radians, and 1.0 radians, the trends were analogous to the two other testing modes (tension, compression). Object count, number density, area fraction, and mean area all showed an increasing trend, while mean nnd produced a decreasing trend. Object count generated values of 49.11 ± 31.99 for 0.8 radians, 124.22 ± 82.04 for 0.9 radians, and 160.22 ± 37.82 radians. Number density generated values of $1.59 \times 10^{-4} \pm 3.09 \times 10^{-4}$ /μm^2 for 0.8 radians, $4.96 \times 10^{-4} \pm 1.09 \times 10^{-3}$ /μm^2 for 0.9 radians, and $6.03 \times 10^{-4} \pm 8.34 \times 10^{-4}$ /μm^2 for 1.0 radians. Area Fraction generated values of 0.00275 ± 0.002 μm^2 for 0.8 radians, 0.00839 ± 0.0064 μm^2 for 0.9 radians, and 0.0120 ± 0.0048 μm^2 for 1.0 radians. Mean Area generated values of 42.135 ± 7.624 for 0.8 radians, 49.024 ± 9.72 for 0.9 radians, and 58.638 ± 12.33 for 1.0 radians. Mean nnd generated values of 79.91 ± 41.354 μm for 0.8 radians, 44.94 ± 20.11 μm for 0.9 radians, and 36.26 ± 3.20 μm for 1.0 radians.
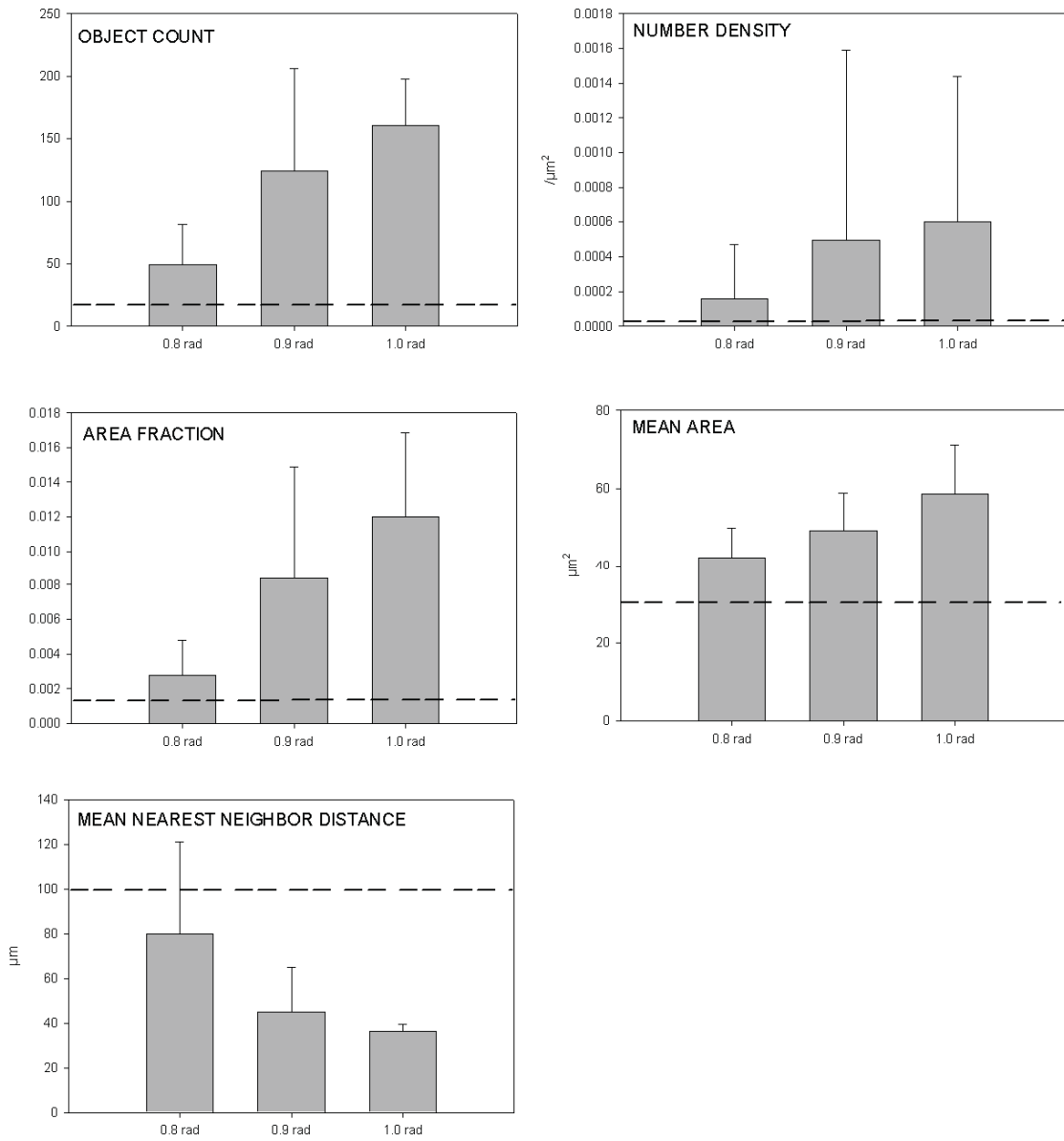
Figure 33 Representative   bar   chart   of   ImageAnalyzer   parameters   for
histological images of tensile interruption tests
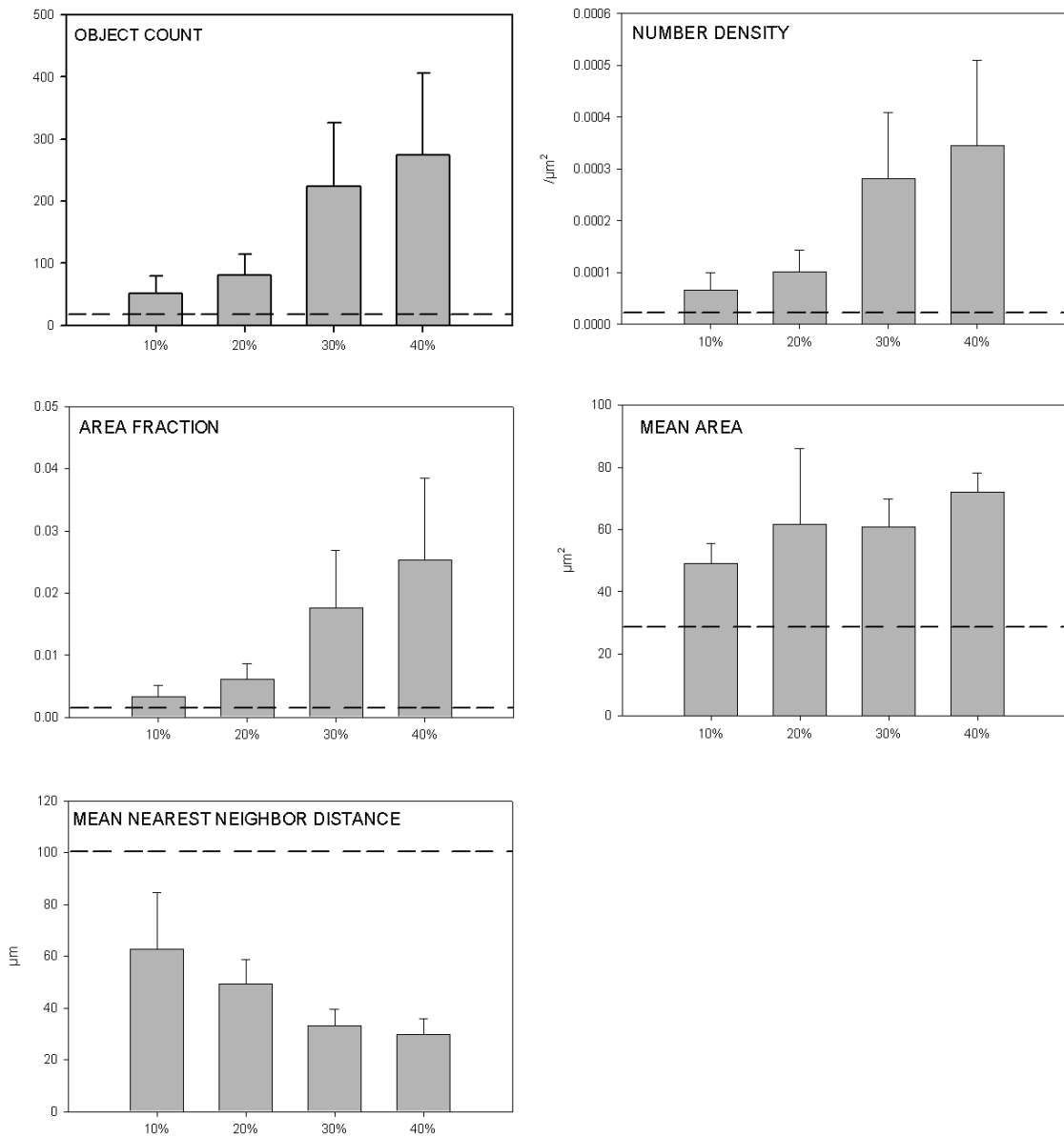
Figure 34   Representative   bar   chart   of   ImageAnalyzer   parameters   for histological images of compression interruption tests
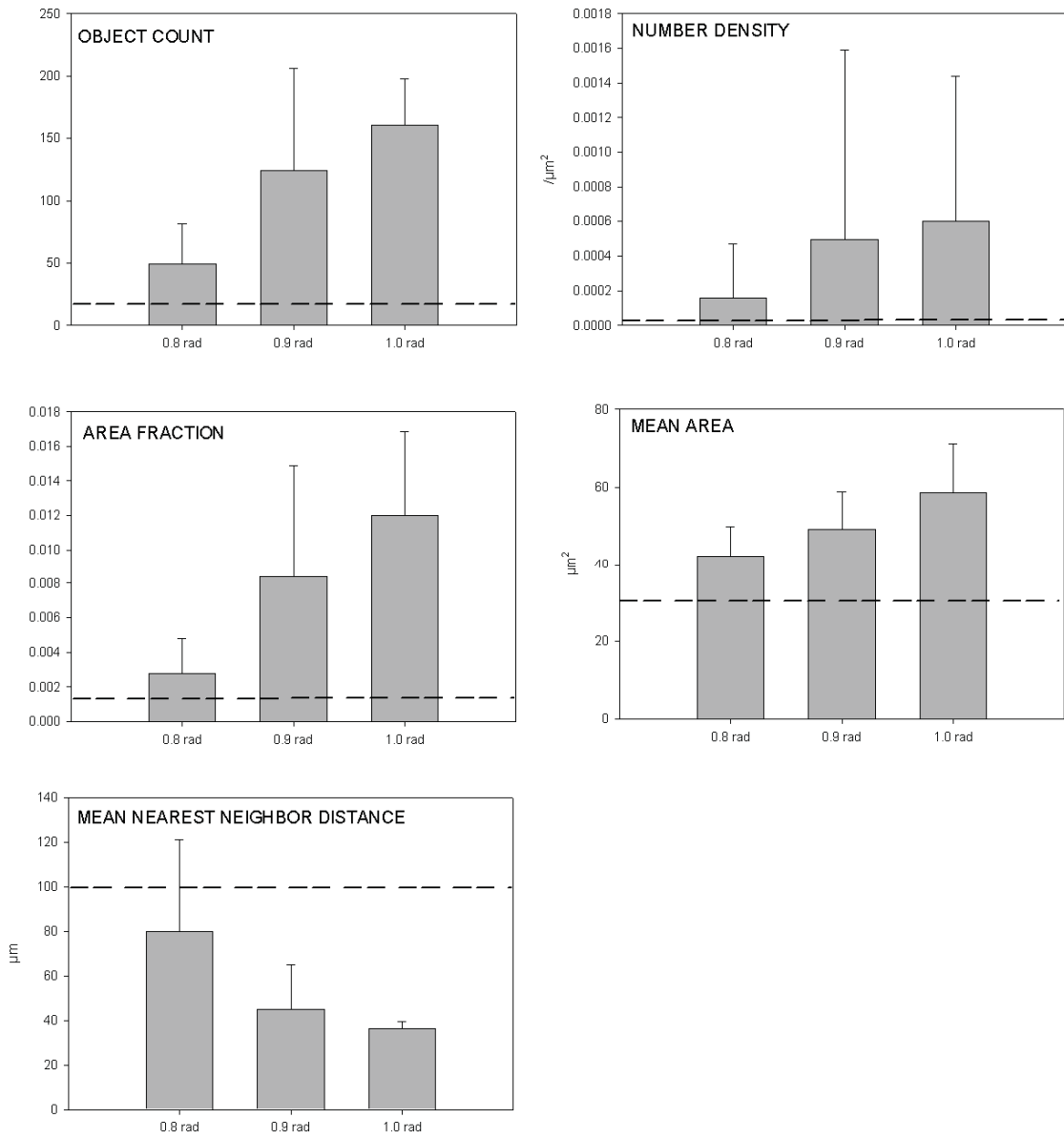
Figure 35   Representative bar chart of ImageAnalyzer parameters for histological images of shear interruption tests

3.4 Discussion

In the most qualitative way, one can see a distinct progression of voids (tissue damage) in the histology images. Quantitatively, we are able to formulate parameters that will be useful in constitutive and FE models. For each of the three testing modes (tension, compression, shear), with increasing strain we see an increase in object count, number density, area fraction, and mean area; we see a decrease in mean nnd with increasing strain. Object count and number density are related because object count is simply referring to the number of voids while number density is referring to the number of voids per area of the image. As strain is increasing, both of these parameters increase because there are more damage being generated. As voids increase, area fraction increases because it represents the area of the voids per area of the image. Mean area refers to the area of the voids. The significant increase of mean area shows that there is not just an increase in void number, but the voids are actually increasing in size as well. The decrease of mean nnd shows that there is a smaller distance between voids as a result of more void generation and size increase of existing voids. These parameters show that as strain increases, these voids increase in both number and size. This type of failure is termed growth dominated failure.

It is interesting to note that the majority of damage and voids are located in the liver lobule; Figure 36 displays the organization of the liver lobules. The connective tissue found between adjacent lobules is in most cases unaltered.
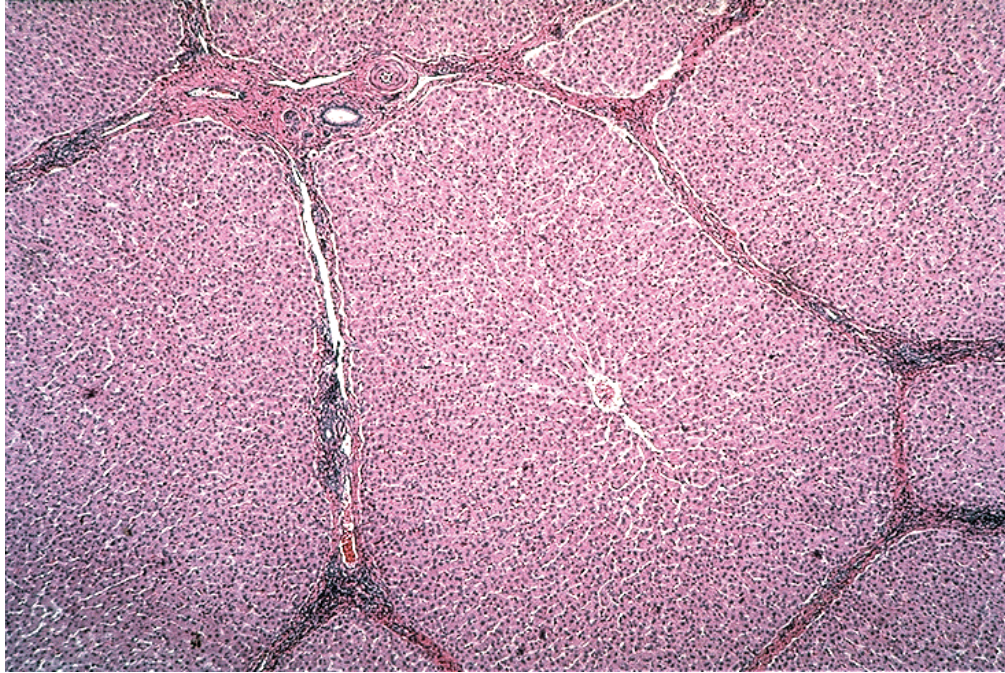
Figure 36   Organization of liver lobules in porcine; From (KMU)

This is the case for all three testing modes. The phenomenon can be described by

the structural makeup of the liver and the contributions of the hepatic ECM. The liver

tissue is composed of many lobules separated by a string of connective tissue, primarily

collagen. In these lobules, there are different components designed to slow down blood

flow to allow the liver cells to filter and clean the blood; however, there is little structural

support. The load bearing element of the liver is probably collagen, but not aligned or

densely packed collagen, but rather a loose network. This network of collagen is easily

compromised when compared to the connective tissue that is lining the lobules; therefore,

in each loading mode (tension, compression, shear), the damage occurs in the lobules

first.   As load increases, these voids increase because they have already been

compromised, and in some cases the damage extends outside the lobule into the connective tissue. The liver is not a homogenous material and therefore the damage occurs at the weaker materials first (lobules) and then the stronger materials (connective tissue).

This failure pattern has been observed for all three testing modes. Tension exhibits the most pronounced void growth and subsequent failure. This is clinically observed because liver lacerations have been attributed to tensile stresses. As the tensile stress builds, less and less intact collagen remains until the rest of the collagen network fails. The shear tests reveal void formation in the lobules along the shearing direction, but the voids are smaller than that of tension. It is possible that this is because shearing is pulling the collagen network at an angle and not directly perpendicular to the surface as it is in tension tests. The compression tests show the same trends, but to a much lesser degree. In compression, the collagen in the ECM serves less of a purpose. It could be that the other ECM components, together of trapped fluids, bear load; therefore allowing the liver to be less "damaged". In cartilage proteoglycan aggregates and bounded water bear much of the repetitive compressive loads, and the proteoglycans in the liver ECM may also serve a similar purpose.

For damage modeling, data from these parameters can be used to generate curves which describe the progression of damage via number density, area fraction, mean area, and, mean nearest neighbor distance. Constitutive equations can be formulated to match these curves and subsequently be inputted in FE models. The micro-level damage progression can be further analyzed to better understand the mechanisms involved in failure.

78

3.5 Conclusion

One major limitation of current FE simulations for automobile accidents is the lack of understanding of true threshold criteria. In the past, damage has been estimated via trial and error based tests, and it has not been objectively analyzed. Presently, force thresholds are set by the Federal Motor Vehicle Safety Standard based on cadaver, animal, and dummy testing. These tests involve subjecting a specimen, for example a cadaver, to a certain amount of force and evaluating the post impact situation. The conclusions are made by the condition of the specimen after the impact. At various speeds of impacts, there will be a different amount of apparent damage. From large lacerations to the vital organs at high speeds to minimal damage at lower speeds, researchers hypothesize a threshold of force that is acceptable for humans to endure. In reality, understanding damage requires more than just force thresholds, it involves the investigation of deformations and their relationship with the progression of tears and voids. By analyzing what is structurally occurring with increasing deformation, researchers can more objectively conclude a threshold deformation and develop methods to prevent the deformation from occurring. In this way, new and improved safety measures can be produced.

A limitation of the study includes the physiological aspect of damage. Although there is clear, objective images allowing us to see how voids are appearing with respect to strain, we cannot predict how the damage affects the liver in the physiological sense. Voids may alter the functionality of the liver, thereby causing even fatal consequences; however, we cannot know for certain by only using interruption tests. Animal studies involving *in vivo* biomechanical stimulation of the liver could be a future avenue for this

type of research. By utilizing a living specimen, researchers could be able to quantify the effects of certain deformations placed on the liver. Nonetheless, the damage/void correlation with strain levels presented in this study is still valuable for the progression of this research.

3.6 Discussion and Future Study

In this study, our goal was to establish an approach to quantify damage in the objective sense by utilizing a novel interruption testing mode. The interruption testing allows researchers to see the progression of voids with increasing strain. This is an important feature in that it provides quantitative data that is available for simulation, modeling, and manipulation. With this approach, damage models can be generated that can produce more accurate threshold criterion for models of high impact situations. Generally, this method is a simple way to generate valuable data. We feel that this is a start in establishing a simple methodology for analyzing the damage evolution in various tissues.

CHAPTER IV

SUMMARY AND CONCLUSIONS

4.1 Major Findings and Improvements

Prevention of injury and/or death related to automobile accidents has been sought

after ever since automobiles began to be integrated into human society. With driving

being an integral part of our everyday lives, the impact of improved safety in automobiles

is apparent. Although car safety today is much improved from years past, automobile

accidents still account for many deaths annually worldwide.

The history of the science of automobile accidents shows that many efforts were

placed on understanding the effects of automobile accidents on the body and how much

force the body could withstand. Although this research has progressed far and many

sophisticated dummies were created from a long history of research and experiments,

there are clear limitations and areas of improvement that can be made today. Improving

automobile safety requires a more detailed examination of the impacts that occur and a

clearer understanding as to how the human body, along with its organs, respond to these

impacts.

This thesis work aims to contribute to the daunting task of creating meaningful,

highly accurate FE models of the human body. As mentioned beforehand, there are three

specific aims summarized in this thesis: *Specific Aim 1: Accurately assess the liver organ*

by using high strain rate mechanical testing, Specific Aim 2: offer an approach for quantifying damage by utilizing interruption testing and histological analysis, and Specific Aim 3: establish methodologies for high strain rate biomechanics and damage evolution modeling. Each specific aim will be revisited and discussed.

Specific Aim 1: Accurately assess the liver organ by using high strain rate mechanical testing. The need for an accurate assessment of soft tissue under high strain rates is apparent when considering the strain rate sensitivity of soft tissues. Y. C. Fung's fundamental book on biomechanics, "Biomechanics: Mechanical Properties of Living Tissues", describes that with increasing strain, there is a stiffening response of the soft tissue [63]. As tissues respond differently under different loading speeds, a tissue impacted under high strain rates would generate different stress-strain curves than a tissue impacted at low strain rates.

In FE modeling, a simple paradigm with respect to methodology is experimental data → constitutive equations → FE simulation. Therefore, in order to generate an accurate simulation, one must have an accurate constitutive equation that describes the phenomenon under investigation, but in order to have an accurate constitutive equation, one must have accurate experimental data. As a result of this cascade, we realize that the issue that is the most important is the experimental data.

We approached this problem with the application of the Split Hopkinson Pressure Bar for high strain analysis. Although the Split Hopkinson Bar has been applied to metals for many years and is established in the field of mechanics, it has not been applied much to soft biological tissues. There have only been a few research groups who have applied the SPHB to soft tissues. Because of the infancy of this type of testing, there

82

were many conclusions presented from the different research groups that were contrary to some of our views. The issues include: inertia effect and the 1-D assumption. As previously stated, the initial stiffness in the high rate stress strain curves has been attributed to inertial effect by various research groups; however, we believe that it is actually a real response regulated by the structural and compositional makeup of the samples as they are being deformed at high rates. The research by Clemmer et al. confirms our hypothesis by comparing high rate responses of brain, liver, and tendon at either hydrated or dehydrated status.

The 1-D assumption of the SHPB test is another issue that must be further investigated to determine its affect on the accuracy of the test. As previously mentioned, the spongy nature of soft tissues when compared to metals results in a different deformation that may or may not negate the 1-D assumption of these tests. Further evaluation of these issues will help discern the accuracy of the SHPB when applied to soft tissues.

Specific Aim 2: offer an approach for quantifying damage by utilizing interruption testing and histological analysis. Revisiting the discussion on the limitations of current safety testing methodology, accepted threshold criterions are limited in their accuracy and can be optimized. Because there is not a thorough understanding of damage, it is difficult to speculate threshold values because there is not detailed objective data to support the assumptions. Although, threshold values are hypothesized with some objective approach, the available data has many shortcomings.

As previously discussed, researchers in the past approached assigning threshold values from a cause and effect standpoint. This approach does not produce an accurate

analysis of the injury occurring, but merely a subjective determination of apparent damage, e.g lacerations. Our approach using interruption testing allows for an objective analysis of voids with increasing strain, giving us a detailed examination of what is occurring at the structural level.

With respect to the specific aim of offering an approach for quantifying damage, we feel that this method succeeds. It is a simple, effective way of investigating the microstructural change that is involved as strains/deformations increase. The image analysis software allows for excellent quantitative characterization, and the potential modeling of these parameters makes this method very valuable. One major limitation could be the quasi static testing approach for these tests. Just as strain rate affects the mechanical response of soft tissues, it could also affect the way voids/damage progresses in a structural way.

Specific Aim 3: establish methodologies for high strain rate biomechanics and damage evolution modeling. In terms of establishing a methodology for any type of research, much time and effort need to be placed on validating the protocol to guarantee that it will produce accurate data. Furthermore, many other research groups should reevaluate these protocols to determine if the data is reproducible. For high strain biomechanics, the methodology, although acceptable, still has room for improvement. With regards to the damage characterization tests via interruption testing, it seems that the protocol is fairly straightforward and can be integrated into conventional biomechanical testing. As there are few issues and problems that arise from this testing approach, we feel that interruption testing will be a good way to characterize how soft tissues damage/fail. There are many benefits to having damage/voids analysis with

increasing strain levels for quasi static scenarios. Furthermore, the damage modeling potential as a result of these tests could prove to be extremely useful.

To summarize, the need for a testing procedure for high strain biomechanics of soft tissue is obvious; therefore, the importance and priority placed on this type of test will become great in the near future. As for interruption testing, we feel that this testing approach produces valuable data and will be adopted by various research groups in the future.

4.2 Future Work

Meaningful human body simulations that can predict damage in high impact scenarios such as automobile accidents are greatly desired because of their potential betterment of the safety features in automobiles. With a better understanding of the response of the human body under these high impact scenarios, optimized safety features will be available that may be able to greatly reduce the number of fatalities associated with automobile accidents.

With our high strain rate biomechanical tests, we aimed to accurately characterize the tissues by addressing the strain rate sensitivity nature of soft tissues. We explored the feasibility of utilizing the SHPB to characterize porcine liver tissue and aspired to establish the SHPB as a potential method to describe the response of soft tissue at high strain rates. We ran 80+ tests using this machine and obtained data that was used to construct stress-strain curves. The integrity of soft tissues differ greatly from metals and therefore a new, thorough investigation of these testing conditions must be done before a

clear validation of the SHPB is possible. We are in the process of evaluating different modeling techniques and parameters to address these issues.

Concerning the efforts to quantify damage, we aimed to use our interruption approach to evaluate the void progression of porcine liver as we increased the strain level. We also hoped to establish this method as an approach to quantify damage evolution in all soft tissues. The data obtained showed good consistency and distinct trends with increasing strain. The only apparent concern was the strain rate sensitivity of the damage progression (quasi static vs high strain).

Future work includes the modeling of the damage using the parameters generated by the image analysis software. We will continue this research by implementing the data into an FE simulation and ultimately applying that model into the human body simulation. We also will try to change the interruption testing protocol to accommodate high strain rate testing.

REFERENCES

1. Margie Peden, R.S., David Sleet, Dinesh Mohan, Adnan A. Hyder, Eva
    Jarawan, Colin Mathers, *World report on road traffic injury prevention*.
    2004, World Health Organization: Switzerland.

2. Mokdad, A.H., et al., *Actual causes of death in the United States, 2000*.
    JAMA, 2004. **291**(10): p. 1238-45.

3. *FARS Data Tables*, N.H.T.S. Administration, Editor. 1994-2008, Fatality
    Analysis Reporting System Encyclopedia.

4. *Mary Ward 1827-1869*, in *Famous Offaly People*2006, Offaly Historical
    & Archaeological Society

5. Dimeo-Ediger, W., *Saved By the Belt*, in *National Geographic*. 2009,
    National Geographic Society.

6. K. U. Schmitt, P.N., F. Walz, *Introduction*, in *Trauma biomechanics:
    introduction to accidental injury*. 2004, Springer-Verlag Berlin
    Heidelberg.

7. *Larry Patrick, pioneer auto safety researchers: 1920 - 2006*, in *News
    Room*. 2006, Wayne State University, College of Engineering.

8. Shashi M. Kuppa, G.S.K., Jeff R. Crandall, Greg Hall, N. Yoganadan, F.
    A. Pintar, Rolf H. Eppinger, Emily Sun, Nopporn Khaewpong, Michael
    Kleinberger, *Axial Impact Characteristics of Dummy and Cadaver Lower
    Limbs*. National Highway Traffic Safety Administration, 1998. **98-S7-O-
    10**: p. 1608-1617.

9. Hardy, W.N., et al., *A study of the response of the human cadaver head to
    impact*. Stapp Car Crash J, 2007. **51**: p. 17-80.

10. News, B., *How the dead have helped the living*, in *BBC News*. 1998, BBC
    News: UK.

11. King, A.I., et al., *Humanitarian benefits of cadaver research on injury
    prevention*. J Trauma, 1995. **38**(4): p. 564-9.

12. Roach, M., *I was a human crash-test dummy*, in *Salon*. 1999, Salon Media Group.

13. Bellis, M., *The History of Crash Test Dummies*, in *The New York Times*: New York, NY.

14. Foster, J.K.K., James O; Wolanin, Michael J, *Hybrid Iii--A Biomehanically-Based Crash Test Dummy.* Society of Automotive Engineers, 1977.

15. *Crash Test Dummies*. 2010 [cited 2010 June 11].

16. Backaitis, S.H.M., Harold J, *Hybrid III: The First Human-Like Crash Test Dummy.* Society of Automotive Engineers, 1993: p. 830.

17. Mello, T.B. *Meet the Family of Crash Test Dummies*. [cited 2010.

18. Cappon, H., et al., *Development and Evaluation of a New Rear-Impact Crash Dummy: The RID 2.* Stapp Car Crash J, 2001. **45**: p. 225-38.

19. Bostrom, O., et al., *Comparison of car seats in low speed rear-end impacts using the BioRID dummy and the new neck injury criterion (NIC).* Accid Anal Prev, 2000. **32**(2): p. 321-8.

20. *Laws & Regulations*, N.H.T.S. Administration, Editor. 2010.

21. Viano, D.C., *Limits and challenges of crash protection.* Accid Anal Prev, 1988. **20**(6): p. 421-9.

22. Pelosi, G., *The finite-element method, Part I: R. L Courant.* Antennas and Propagation Magazine, IEEE, 2007. **49**(2): p. 180-182.

23. Strang, G.F., George, *An Analysis of the Finite Element Method*, ed. Wellesley-Cambridge. 1973.

24. *ABAQUS/Explicit User's Manual, Version 6.9*. 2009, Hibbit, Karlsson, and Sorenson, Inc.: Providence, RI.

25. Reddy, J.N., *An Introduction to the Finite Element Method.* 2005: Tata McGraw-Hill

26. Rush, C., *Crash Testing: Using Computers to Save Livers.* International Journal of Trauma Nursing, 2000. **6**: p. 61-63.

27. King, A.I. and C.C. Chou, *Mathematical modelling, simulation and experimental testing of biomechanical system crash response.* J Biomech, 1976: p. 301-17.

28. Kirkpatrick, S.M., Robert; Bocchieri, Robert, *Development of an LS-DYNA Occupant Model for use in Crash Analyses of Roadside Safety Features.* 2002. **03-4450**.

29. Deng, Y.C., *Anthropomorphic dummy neck modeling and injury considerations.* Accid Anal Prev, 1989. **21**(1): p. 85-100.

30. R. Jost, G.N.N., *Finite Element modelling of the human body in vehicle side impact.* International Journal of Crashworthiness, 1999. **4**(1): p. 31-37.

31. Jay Zhao, G.N., *Development of a Human Body Finite Element Model For Restraint System R&D Applications.* 2004. **05-0399**: p. 1-13.

32. Dirk Fressmann, T.M., Oliver Graf, Karl Schweizerhof, *FE Human Modelling in Crash - Aspects of the numerical modelling and current applications in the automotive industry.* 2007: p. 1-23.

33. Feliciano, D.V., *Surgery for liver trauma.* Surgical Clinics of North America, 1989. **69**: p. 273-284.

34. Feliciano, D.V. and G.S. Rozycki, *The management of penetrating abdominal trauma.* Adv Surg, 1995. **28**: p. 1-39.

35. Gilday, D.L. and P.O. Alderson, *Scintigraphic evaluation of liver and spleen injury.* Semin Nucl Med, 1974. **4**(4): p. 357-70.

36. Iuchtman, M., et al., *Mesh wrap in severe pediatric liver trauma.* J Pediatr Surg, 2004. **39**(10): p. 1485-9.

37. Lester F. Williams Jr, J.J.B., *Trauma to the Liver at the Boston City Hospital from 1955 to 1965.* American Journal of Surgery: p. 368-375.

38. Jackie Springer, A.C., *A traumatic car crash.* Lancet, 2001. **357**: p. 1848.

39. Guyton, A.C.H., John E, *Textbook of Medical Physiology*. 2000: W.B. Saunders Compnay. 1064.

40. Viano, D.C., et al., *Biomechanics of the human chest, abdomen, and pelvis in lateral impact.* Accid Anal Prev, 1989. **21**(6): p. 553-74.

41. Viano, D.C., et al., *Injury biomechanics research: an essential element in the prevention of trauma.* J Biomech, 1989. **22**(5): p. 403-17.

42. Elhagediab, A.M., Rouhana, R. B. *Patterns of abdominal injury in frontal automotive crashes*. in *16th International ESV Conference Proceedings, NHTSA*. 1998. Washington, DC.

43.   Rouhana, S.W., Foster, M. E. *Lateral impact—an analysis of the statistics in the NCSS*. in *Proceedings of the 29th Stapp Car Crash Conference, Society of Automotive Engineers*. 1985. Warrendale, PA.

44.   O'Neill, B., *Preventing passenger vehicle occupant injuries by vehicle design—a historical perspective from IIHS* Traffic Injury Prevention, 2009. **10**(2): p. 113-126.

45.   Mertz, H., *Injury assessment reference values used to evaluate Hybrid III response measurements.* General Motors Submission, 1984.

46.   Mertz, H.P., P; Irwin, Al, *Injury risk curves for children and adults in frontal and rear collisions.* SAE, 1997.

47.   Deng, Y.-C., Kong, W., Ho, H. *Development of a finite element human thorax model for impact injury studies*. in *SAE Technical Paper Series, 1999-01-0715*. 1999.

48.   Haug, E. *Biomechanical models in vehicle accident simulation*. in *Proceedings of the 1996 NATO Advanced Study Institute on Crashworthiness of Transportation Systems: Structural Impact and Occupant Protection*. 1997. Tro´ ia, Portugal.

49.   Iwamoto, M., Kisanuki, Y., Watanabe, I., Furusu, K., Miki, K. *Development of a finite element model of the total human model for safety (THUMS) and application to injury protection*. in *Proceedings of the 2002 International Conference on the Biomechanics of Impact*. 2002. Munich, Germany.

50.   Kimpara, H., Iwamoto, M., Miki, K., Lee, J.B., Begeman, P., Yang, K.H., King, A.I., *Biomechanical properties of the male and female chest subjected to frontal and lateral impacts*, in *2003 International IRCOBI Conference on the Biomechanics of Impact*. 2003: Lisbon, Portugal.

51.   Song, B., et al., *Dynamic and quasi-static compressive response of porcine muscle.* Journal of Biomechanics, 2007. **40**(13): p. 2999-3005.

52.   Van Sligtenhorst, C., D.S. Cronin, and G. Wayne Brodland, *High strain rate compressive properties of bovine muscle tissue determined using a split Hopkinson bar apparatus.* Journal of Biomechanics, 2006. **39**(10): p. 1852-1858.

53.   Cheung, J.B. and C.C. Hsiao, *Nonlinear anisotropic viscoelastic stresses in blood vessels.* J Biomech, 1972. **5**(6): p. 607-19.

54.   del Palomar, A.P., B. Calvo, and M. Doblare, *An accurate finite element model of the cervical spine under quasi-static loading.* J Biomech, 2008. **41**(3): p. 523-31.

55.   Mohan, D. and J.W. Melvin, *Failure properties of passive human aortic tissue. I--uniaxial tension tests.* J Biomech, 1982. **15**(11): p. 887-902.

56.   Yingling, V.R., J.P. Callaghan, and S.M. McGill, *Dynamic loading affects the mechanical properties and failure site of porcine spines.* Clin Biomech (Bristol, Avon), 1997. **12**(5): p. 301-305.

57.   Sparks, J. and R. Dupaix, *Constitutive modeling of rate-dependent stress–strain behavior of human liver in blunt impact loading.* Annals of Biomedical Engineering, 2008. **36**(11): p. 1883-1892.

58.   Bazle A Gama, S.L.L., John W Gillespie Jr, *Hopkinson bar experimental technique: A critical review.* Appl Mech Rev, 2004. **57**(4): p. 223-250.

59.   M.J. Forrestal, T.W.W., W. Chen, *The effect of radial inertial on brittle samples during the split Hopkinson pressure bar test.* International Journal of Impact Engineering, 2007. **34**: p. 405-411.

60.   R. J. Christensen, S.R.S., W. S. Brown, *Split-Hopkinson-bar Tests on Rock under Confining Pressure.* Experimental Mechanics, 1972: p. 508-513.

61.   Salisbury, C., *Spectral analysis of wave propagation through a polymeric Hopkinson bar.* 2001, University of Waterloo.

62.   Zhao, H., Gary, G., *On the use of a viscoelastic split Hopkinson pressure bar.* International Journal of Impact Engineering, 1997. **19**(4): p. 319-330.

63.   Fung, Y.C., *Biomechanics: Mechanical Properties of Living Tissues*. 2nd ed. 1993, New York, NY: Springer.

64.   Snedeker, J.G., et al., *Strain-rate dependent material properties of the porcine and human kidney capsule.* Journal of Biomechanics, 2005. **38**(5): p. 1011-1021.

65.   Roan, E., Vemaganti, K., *The nonlinear material properties of liver tissue determined from no-slip uniaxial compression experiments.* Journal of Biomechanical Engineering, 2007. **129**: p. 450-456.

66.   Saraf, H., et al., *Mechanical properties of soft human tissues under dynamic loading.* Journal of Biomechanics, 2007. **40**(9): p. 1960-1967.

67.   Bouvard, J.L., Brown, H.R., Marin, E.B., Wang, P. and Horstemeyer, M.F. *Mechanical Testing and Material Modeling of Thermoplastics: Polycarbonate, Polypropylene and Acrylonitrile-Butadiene-Styrene*. in *MRS Fall Symposium W 2009*. 2009.

68.   Song, B., Chen, W., *Dynamic stress equilibration in split Hopkinson pressure bar tests on soft materials.* Experimental Mechanics, 2004. **44**(3): p. 300-312.

69.   Sakuma, I., et al., *In vitro Measurement of Mechanical Properties of Liver Tissue under Compression and Elongation Using a New Test Piece Holding Method with Surgical Glue* in *Surgery Simulation and Soft Tissue Modeling*, N. Ayache and H. Delingette, Editors. 2003, Springer Berlin / Heidelberg. p. 284 - 292.

70.   Liying, Z., H.Y. King, and I.K. Albert, *A Proposed Injury Threshold for Mild Traumatic Brain Injury.* Journal of Biomechanical Engineering, 2004. **126**(2): p. 226-236.

71.   Newman, J.A., N. Shewchenko, and E. Welbourne, *A proposed new biomechanical head injury assessment function - the maximum power index.* Stapp Car Crash J, 2000. **44**: p. 215-47.

72.   Baker, A.R., E.P. Perry, and D.P. Fossard, *Traumatic rupture of the stomach due to a seat belt.* Injury, 1986. **17**(1): p. 47-48.

73.   Horgan, T.J. and M.D. Gilchrist, *Influence of FE model variability in predicting brain motion and intracranial pressure changes in head impact simulations.* International Journal of Crashworthiness, 2004. **9**(4): p. 401 - 418.

74.   Jakeman, L.B., et al., *Traumatic spinal cord injury produced by controlled contusion in mouse.* J Neurotrauma, 2000. **17**(4): p. 299-319.

75.   Kleiven, S. and W.N. Hardy, *Correlation of an FE Model of the Human Head with Local Brain Motion--Consequences for Injury Prediction.* Stapp Car Crash J, 2002. **46**: p. 123-44.

76.   Mao, H., et al., *Application of a finite element model of the brain to study traumatic brain injury mechanisms in the rat.* Stapp Car Crash J, 2006. **50**: p. 583-600.

77.   Miller, K., *Constitutive modelling of abdominal organs.* Journal of Biomechanics, 2000. **33**(3): p. 367-373.

78.   Richens, D., et al., *A finite element model of blunt traumatic aortic rupture.* Eur J Cardiothorac Surg, 2004. **25**(6): p. 1039-1047.

79. Snedeker, J.G., et al., *The creation of a high-fidelity finite element model of the kidney for use in trauma research.* The Journal of Visualization and Computer Animation, 2002. **13**: p. 53-64.

80. Tropiano, P., et al., *Using a Finite Element Model to Evaluate Human Injuries Application to the HUMOS Model in Whiplash Situation.* Spine, 2004. **29**(16): p. 1709-1716.

81. Nahum, A.M.M., John W., *Accidental Injury Biomechanics and Prevention*. 2002, New York: Springer - Verlag.

82. Kim, J., et al., *An efficient soft tissue characterization algorithm from in vivo indentation experiments for medical simulation.* Int J Med Robot, 2008. **4**(3): p. 277-85.

83. Liu, Z. and L.E. Bilston, *Large deformation shear properties of liver tissue.* Biorheology, 2002. **39**(6): p. 735-42.

84. Miller, K., *Method of testing very soft biological tissue in compression.* Journal of Biomechanics, 2005. **38**: p. 153-158.

85. Roan, E. and K. Vemaganti, *The nonlinear material properties of liver tissue determined from no-slip uniaxial compression experiments.* J Biomech Eng, 2007. **129**(3): p. 450-6.

86. Sakuma, I., Nishimura, Y., Chui, C.K., Kobayashi, E., Inada, H., Chen, X., Hisada, T., *In vitro Measurement of Mechanical Properties of Liver Tissue under Compression and Elongation Using a New Test Piece Holding Method with Surgical Glue.* LNCS, 2003: p. 284-292.

87. Stingl, J., et al., *Morphology and some biomechanical properties of human liver and spleen.* Surg Radiol Anat, 2002. **24**(5): p. 285-9.

88. Brown, J.D., et al., *In-vivo and in-situ compressive properties of porcine abdominal soft tissues.* Stud Health Technol Inform, 2003. **94**: p. 26-32.

89. Holzapfel, G.A., *Biomechanics of Soft Tissue*, in *Lemaitre Handbook of Materials Behavior Models*. 2001, Academic Press.

90. Hoeve, C.A.J., *The Elastic Properties of Elastin.* Biopolymers, 1974. **13**: p. 677-686.

91. Martinez-Hernandez, A.A., Peter Sebastian, *The extracellular matrix in hepatic regeneration.* FASEB, 1995. **9**: p. 1401-1410.